

~~CONFIDENTIAL~~

UNCLASSIFIED

Copy
RM L54I20

5



RESEARCH MEMORANDUM

EXPERIMENTAL INVESTIGATION AT HIGH SUBSONIC
SPEEDS OF THE ROLLING STABILITY DERIVATIVES OF A COMPLETE
MODEL WITH AN ASPECT-RATIO-2.52 WING HAVING AN UNSWEPT
72-PERCENT-CHORD LINE AND A HIGH HORIZONTAL TAIL

By William C. Sleeman, Jr., and James W. Wiggins

Langley Aeronautical Laboratory
Langley Field, Va.

CLASSIFICATION CHANGED

LIBRARY COPY

To UNCLASSIFIED

MAY 31 1955

By authority of t.P.A. # 17 *effective 3/18/60*
LANGLEY AERONAUTICAL LABORATORY
LIBRARY, NACA
LANGLEY FIELD, VIRGINIA

This material contains information affecting the National Defense of the United States within the meaning of the espionage laws, Title 18, U.S.C., Secs. 793 and 794, the transmission or revelation of which in any manner to an unauthorized person is prohibited by law.

**NATIONAL ADVISORY COMMITTEE
FOR AERONAUTICS**

WASHINGTON

May 26 1955

~~CONFIDENTIAL~~

UNCLASSIFIED

NATIONAL ADVISORY COMMITTEE FOR AERONAUTICS

RESEARCH MEMORANDUM

EXPERIMENTAL INVESTIGATION AT HIGH SUBSONIC
SPEEDS OF THE ROLLING STABILITY DERIVATIVES OF A COMPLETE
MODEL WITH AN ASPECT-RATIO-2.52 WING HAVING AN UNSWEPT
72-PERCENT-CHORD LINE AND A HIGH HORIZONTAL TAIL

By William C. Sleeman, Jr., and James W. Wiggins

SUMMARY

Rolling stability derivatives are presented for a complete model having a low-aspect-ratio wing and tail surfaces for a Mach number range of 0.70 to 0.94 and for an angle-of-attack range from 0° to 13° for the lower Mach numbers. The model had a wing of aspect ratio 2.52, a taper ratio of 0.385, and 19.1° sweep of the quarter chord. The wing airfoil was a modified biconvex section of 3.4-percent-chord thickness having an elliptical nose profile.

The model test results indicated regions of neutral or unstable damping in roll at Mach numbers of 0.85 and 0.90 in the higher angle-of-attack range for the basic model. Addition of wing-tip tanks approximately doubled the damping in roll at low angles of attack and, although large decreases in damping occurred in going to high angles of attack, positive damping was indicated over the range of test conditions for the complete model with tanks. At 0° angle of attack, addition of wing-tip tanks increased the aileron effectiveness of the basic model; however, the rolling angular velocity which could be obtained with a given aileron deflection was decreased about 30 percent by addition of the wing tanks. Deflection of leading-edge flaps, in general, appeared to increase the angle of attack at which large losses in damping in roll occurred.

In addition to the aforementioned damping results, the other rolling derivatives (yawing moment and lateral force due to rolling) were obtained.

INTRODUCTION

A series of tests were made in the Langley high-speed 7- by 10-foot tunnel to determine the rolling stability derivatives of a complete model having a low-aspect-ratio wing and tail. The model had a wing of aspect ratio 2.52, a taper ratio of 0.385, and zero sweep of the 72-percent-chord line (19.1° sweepback of the quarter-chord line). The wing airfoil was a modified biconvex section of 3.4-percent-chord thickness having an elliptical nose profile.

Results are presented for the basic configuration over a Mach number range from 0.70 to 0.94 and for a maximum angle-of-attack range of approximately 0° to 13° . A number of breakdown tests were made to determine the contribution of the tail surfaces to the rolling derivatives of the model with and without the wing. Tests also were made to obtain the effects of wing-tip tanks with ailerons undeflected and deflected. A few tests were made with 92.5-percent-span leading-edge flaps deflected.

Analysis and discussion of the test results have been made brief in order to expedite publication of these data.

COEFFICIENTS AND SYMBOLS

The results of this investigation are presented as standard NACA coefficients of forces and moments referred to the stability system of axes shown in figure 1. Moment coefficients are given with respect to the center-of-gravity location shown in figure 2 (25-percent mean aerodynamic chord on the fuselage center line).

C_l	rolling-moment coefficient, $\frac{\text{Rolling moment}}{qSb}$
C_n	yawing-moment coefficient, $\frac{\text{Yawing moment}}{qSb}$
C_y	lateral-force coefficient, $\frac{\text{Lateral force}}{qS}$
q	dynamic pressure, $\frac{1}{2}\rho V^2$, lb/sq ft
ρ	air density, slugs/cu ft
V	free-stream velocity, ft/sec

M	free-stream Mach number
S	wing area, sq ft
b	wing span, ft
α_u	nominal uncorrected geometric angle of attack of fuselage center line, deg
α	corrected angle of attack of fuselage center line, deg
δ_{aT}	total (or combined) deflection of left and right ailerons, deg
δ_N	leading-edge flap deflection, deg
p	rolling angular velocity, radians/sec
$pb/2V$	wing-tip helix angle, radians
$C_{l_p} = \frac{\partial C_l}{\partial \frac{pb}{2V}}$	
$C_{n_p} = \frac{\partial C_n}{\partial \frac{pb}{2V}}$	
$C_{Y_p} = \frac{\partial C_Y}{\partial \frac{pb}{2V}}$	
$C_{l\delta_{aT}}$	aileron effectiveness per degree total aileron deflection
$(pb/2V)\delta_{aT}$	rolling effectiveness of ailerons per degree total aileron deflection

CONFIGURATION DESIGNATION

W	wing
W_T	wing with tip tanks

F	fuselage
V	vertical tail
H	horizontal tail

MODEL AND APPARATUS

A sketch of the model with pertinent geometric characteristics is given in figure 2, and photographs of the model mounted on the forced-roll sting at 0° and 10° angle of attack are given in figure 3. The model was constructed of steel.

The wing which had 10° of negative dihedral and the tail surfaces could be removed from the fuselage for break-down tests. For these tests, the component parts were replaced by smooth fairing blocks which continued the fuselage contour. The air inlets were faired over as shown in figures 2 and 3 and therefore there was no air flow through the model for the rolling tests.

The model was tested in steady roll on the forced-roll sting support shown schematically in figure 4. For these tests the model was mounted on a 6-component internal strain-gage balance and was rotated about the X-axis of the stability axes. Electrical signals from the strain-gage balance were transmitted to the data-recording equipment by means of wire leads, slip rings, and brushes. (See fig. 4.) The model angle of attack was changed by use of various offset sting adapters (figs. 3 and 4) which were designed to allow the model to rotate about the moment reference center at each angle of attack. Further details of the forced-roll testing technique can be found in reference 1.

TESTS AND CORRECTIONS

Test Conditions

Tests were made in the Langley high-speed 7- by 10-foot tunnel over a Mach number range from 0.70 to 0.94 and through a maximum angle-of-attack range from 0° to approximately 13° . The variations with Mach number of maximum wing-tip helix angle $pb/2V$ and mean test Reynolds number based on the wing mean aerodynamic chord are presented in figure 5.

Corrections

Blockage corrections which were determined by use of the method of reference 2 were applied to the Mach number and dynamic pressure based on usual nonrolling model conditions. Jet-boundary corrections applied to the angle of attack were obtained from reference 3 and corrections for deflection of the model and support system under aerodynamic load also were applied to the angle of attack.

The support system deflected under load and these deflections, combined with any initial displacement of the mass center of gravity of the model from the roll axis, introduced centrifugal forces and moments when the model was rotated. Corrections for these forces and moments were determined and have been applied to these data.

Corrections to the rolling derivatives for jet-boundary effects were not applied to the data, since these corrections were found to be negligible. Corrections for sting tares have not been applied to the data; however, these corrections are believed to be small.

PRESENTATION OF RESULTS

The figures presenting the results are as follows:

	<u>Figure</u>
Rolling Stability Derivatives:	
Wing off	6
Basic model, effect of tail surfaces	7
Basic model with tanks on	8
Effect of leading-edge flap	9
Characteristics with ailerons deflected	10
Aileron effectiveness and rolling power	11
Variation of Lateral Characteristics with $pb/2V$:	
Wing off	12, 13
Wing on, basic model	14, 15, 16
Basic model with tanks on	17
Basic model with leading-edge flaps deflected	18
Configurations with ailerons deflected	19

The basic data of this investigation were obtained as variations of C_l , C_n , and C_y with rolling angular velocity. In most cases these variations were linear over a fairly large range of wing-tip helix angle and for these linear conditions, the derivatives presented apply for the range of values of wing-tip helix angle investigated. Pronounced

nonlinearities were present, however, for some configurations at angles of attack other than 0° and, consequently, the derivatives, which were determined at low values of $pb/2V$, may not be applicable at higher rates of roll. Because several cases of pronounced nonlinear variations with $pb/2V$ were evident, the forces and moments which were used in determining most of the rolling derivatives are presented (figs. 12 to 19). Fairly consistent nonlinearities with $pb/2V$ were in evidence for C_Y and C_n for the various tail-off configurations, whereas corresponding tail-on test results were linear over a fairly large range of $pb/2V$. Reasons for these differences in tail-off and tail-on test results are not known and possible explanations of these differences would be based primarily on conjecture. It is believed however, that the aforementioned nonlinearities were probably caused by effects other than aerodynamic.

DISCUSSION

Damping in Roll

Damping-in-roll results for both the wing-fuselage configuration and the complete model showed similar trends with increasing angle of attack in that an initial increase in damping at low angles was followed by a large reduction at moderately high angles of attack (fig. 7). For the wing-fuselage configuration, regions of unstable damping (positive values of C_{l_p}) were indicated at $M = 0.85$ and $M = 0.90$ in the higher angle-of-attack range. Addition of the tail surfaces effected some reduction in the unstable damping encountered at these Mach numbers; however, the damping in roll of the complete model was still neutral or slightly unstable.

Comparison of figures 7 and 8 indicates that addition of the wing-tip tanks approximately doubled the damping in roll of the basic model at low angles of attack. Although significant losses in damping occurred with increasing angle of attack, positive damping was indicated throughout the test angle-of-attack and Mach number range for the complete model with tanks on (fig. 8). With regard to the effects of tanks and the test data in general at the highest test angle of attack, an overall evaluation of damping results is difficult because of the nonlinear nature of the rolling-moment variation with $pb/2V$ (e.g. fig. 17).

Effects of deflecting the leading-edge flaps on the complete model are shown in figure 9. Because there was essentially no effect on damping in roll at $\alpha = 0^\circ$, only the results at the highest test angles of attack are presented in figure 9. In general, deflection of the leading-edge flaps increased the damping and delayed the abrupt loss in damping for the basic model to higher angles of attack. Unstable damping was

encountered, however, with the leading-edge flaps deflected at a Mach number of 0.90 and at approximately 13° angle of attack.

Yawing Moment and Lateral Force Due to Rolling

A comparison of figures 6 and 7 indicates that the tail contribution to C_{np} and C_{yp} for the wing on is appreciably different from that for the wing-off configuration and this difference is in accord with the side-wash due to roll effect discussed in reference 4.

Effects of modifications to the basic model such as deflection of leading-edge flaps and addition of wing-tip tanks were relatively small with regard to lateral force and yawing moment due to rolling.

Aileron Characteristics

Aileron control characteristics obtained from forced steady roll tests of the complete model are summarized in figure 11 for three angles of attack, and effects of the tail and wing-tip tanks are indicated. Values of damping in roll with ailerons deflected are repeated for convenience in interpreting the results of figure 11. The aileron effectiveness $C_{l\delta_{aT}}$ and rolling effectiveness $(pb/2V)\delta_{aT}$ presented were obtained by assuming that the aileron characteristics were linear between the specific deflections tested (0° and 7.5° for each aileron).

The most significant effects indicated in figure 11 are those associated with addition of the wing-tip tanks. At 0° angle of attack, an increase in aileron effectiveness $C_{l\delta_{aT}}$ of about 50 percent was gained by addition of the tanks to the complete model; however, the value of $pb/2V$ which could be attained with a given aileron deflection with tanks on was decreased about 30 percent. This loss in rolling effectiveness with the tanks on is of course due to the increased damping in roll obtained for this configuration. The aileron effectiveness at an angle of attack of approximately 6.7° with tanks on was not appreciably different from that for the basic model, and the damping was generally somewhat less - which resulted in an increase in $(pb/2V)\delta_{aT}$ with tanks on. Results at the highest angle of attack are presented for completeness; however, nonlinearities in the rolling-moment variation with $pb/2V$ and very low damping in roll considerably decrease the significance of these results.

A rather unusual effect is indicated in figure 11 with regard to effects of the horizontal tail on aileron effectiveness at the highest test angle of attack. At low angles of attack, as would be expected,

addition of the horizontal tail had only a small effect on $C_{l\delta_{aT}}$, whereas addition of the horizontal tail increased $C_{l\delta_{aT}}$ from 50 to 100 percent at the highest angle. A possible explanation of this increased aileron effectiveness may be made by consideration of effects of the vortex shed from the inboard end of the aileron on the horizontal tail. The vortex shed from the inboard end of a downward-deflected aileron, for example, would induce an upload increment on the horizontal tail which would add an increment of rolling moment of the same sense as that produced directly by deflection of the aileron. This vortex effect would be expected to be present for this configuration only at the higher angles of attack where the horizontal tail moves down into the vortex field. It is perhaps of interest to note that the reverse of this effect has been observed on other models having inboard ailerons, for which effects of vorticity shed from the outboard end of the aileron would be expected to predominate and induce an unfavorable rolling-moment contribution of the horizontal tail.

CONCLUDING REMARKS

Test results pertaining to the rolling stability derivatives for a complete model having a low-aspect-ratio wing and tail surfaces indicated regions of neutral or unstable damping in roll at Mach numbers of 0.85 and 0.90 in the higher angle-of-attack range for the basic model. Addition of wing-tip tanks approximately doubled the damping in roll at low angles of attack and, although large decreases in damping occurred in going to high angles of attack, positive damping was indicated over the range of test conditions for the complete model with tanks. At 0° angle of attack, addition of the wing-tip tanks increased the aileron effectiveness of the basic model; however, the rolling angular velocity which could be obtained with a given aileron deflection was decreased about 30 percent by addition of the wing tanks. Deflection of leading-edge flaps in general appeared to increase the angle of attack at which large losses in damping in roll occurred.

Langley Aeronautical Laboratory,
National Advisory Committee for Aeronautics,
Langley Field, Va., September 2, 1954.

REFERENCES

1. Kuhn, Richard E., and Wiggins, James W.: Wind-Tunnel Investigation To Determine the Aerodynamic Characteristics in Steady Roll of a Model at High Subsonic Speeds. NACA RM L52K24, 1953.
2. Hensel, Rudolph W.: Rectangular-Wind-Tunnel Blocking Corrections Using the Velocity-Ratio Method. NACA TN 2372, 1951.
3. Gillis, Clarence L., Polhamus, Edward C., and Gray, Joseph L., Jr.: Charts for Determining Jet-Boundary Corrections for Complete Models in 7- by 10-Foot Closed Rectangular Wind Tunnels. NACA WR L-123, 1945. (Formerly NACA ARR L5G31.)
4. Michael, William H., Jr.: Analysis of the Effects of Wing Interference on the Tail Contributions to the Rolling Derivatives. NACA Rep. 1086, 1952. (Supersedes NACA TN 2332.)

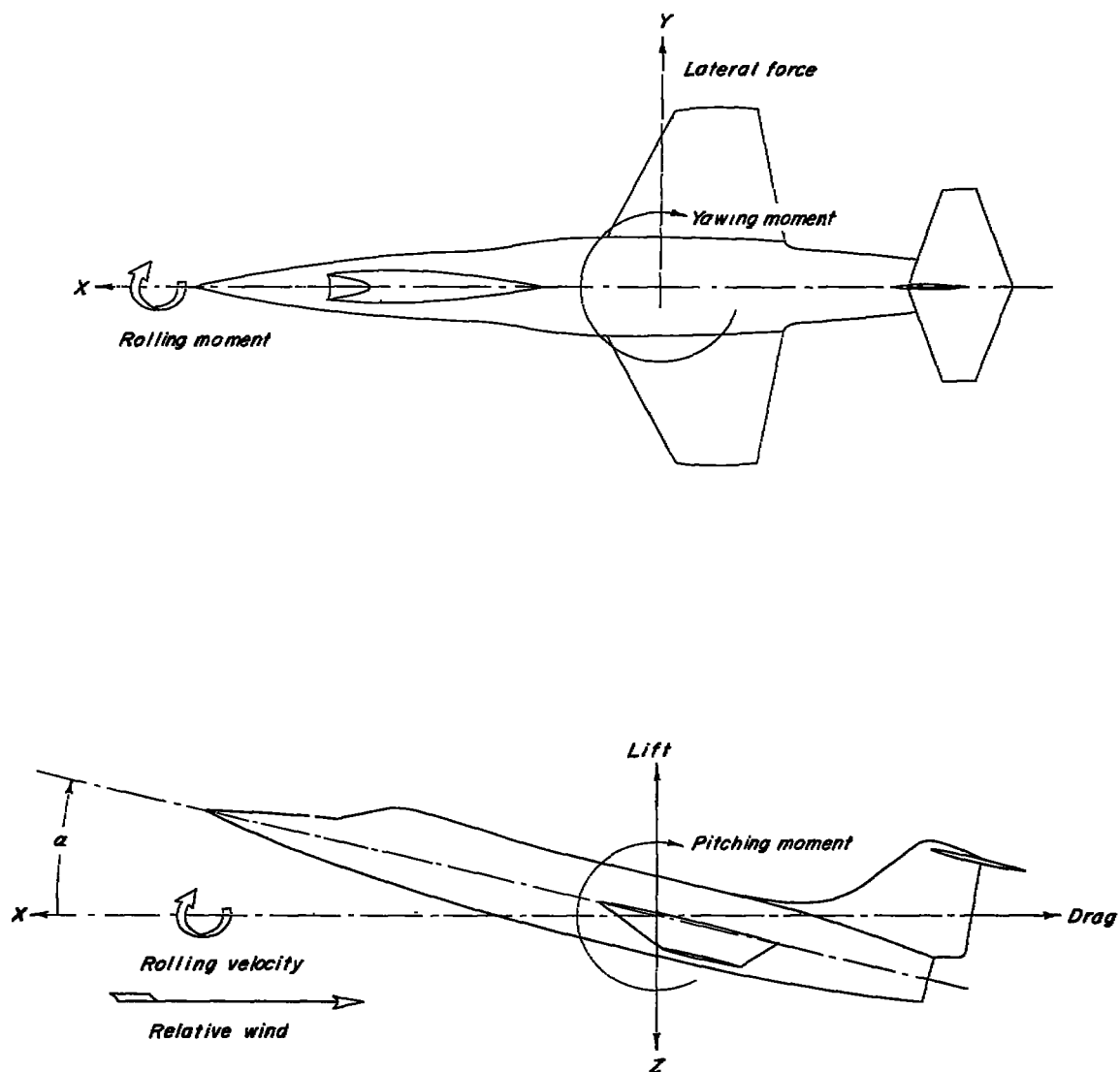


Figure 1.- Stability system of axes used showing positive directions of forces, moments, angles, and velocities.

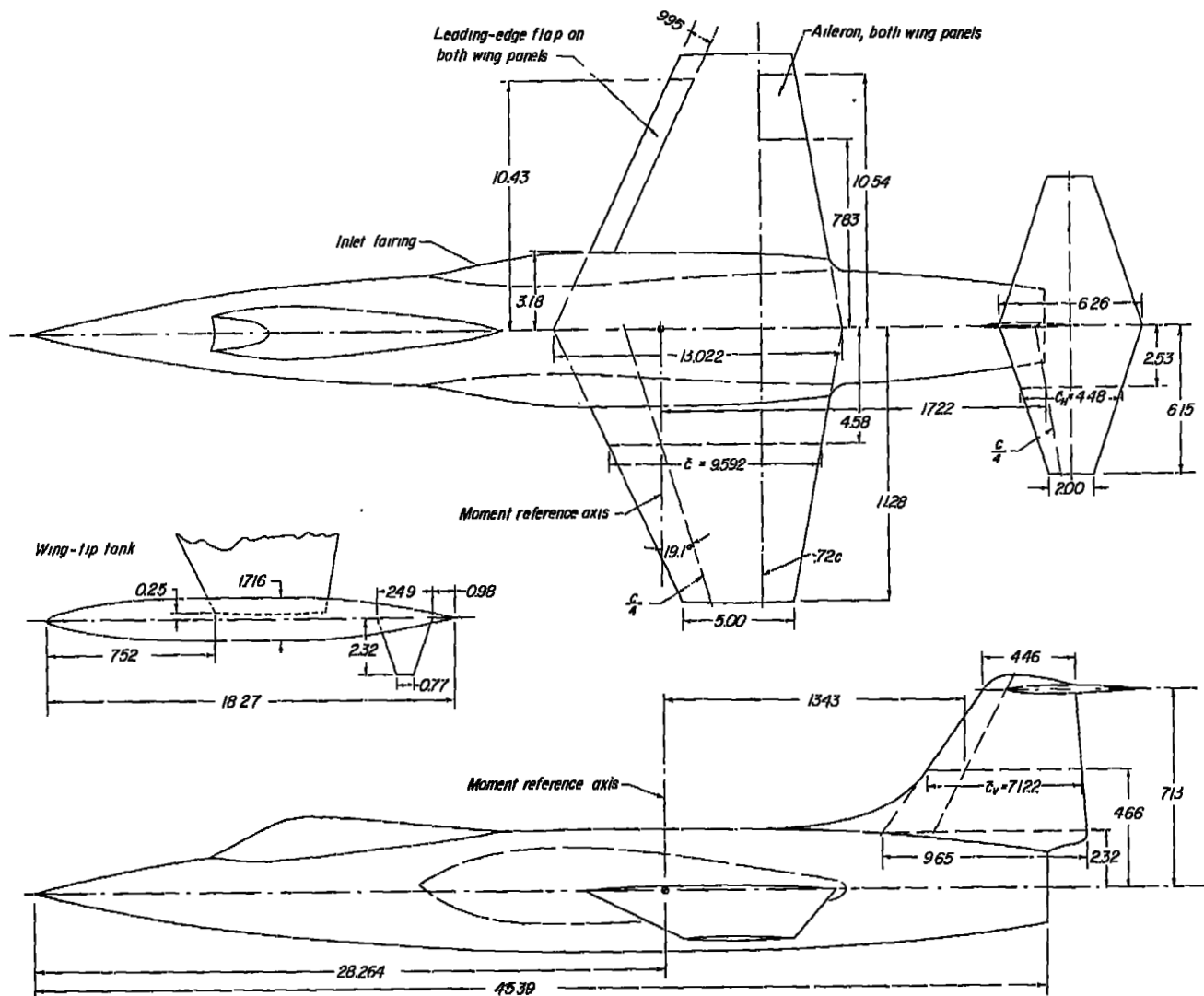


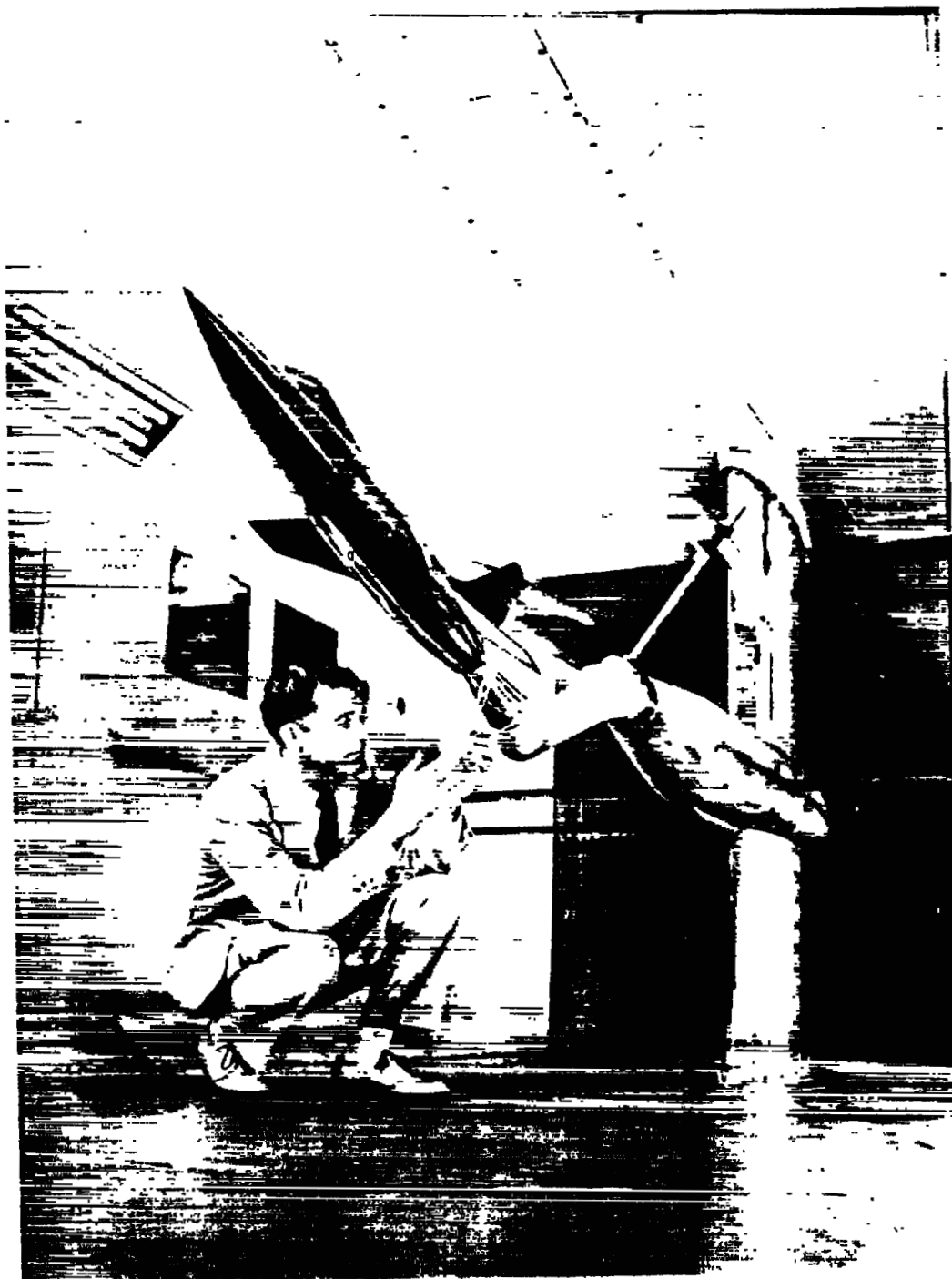
Figure 2.- General arrangement of the complete model tested in the Langley high-speed 7- by 10-foot tunnel.



(a) $\alpha = 0^\circ$.

L-82337

Figure 3.- Photographs of the test model mounted on the forced-roll sting support in the Langley high-speed 7- by 10-foot tunnel.



(b) $\alpha = 10^\circ$.

L-82336

Figure 3.- Concluded.

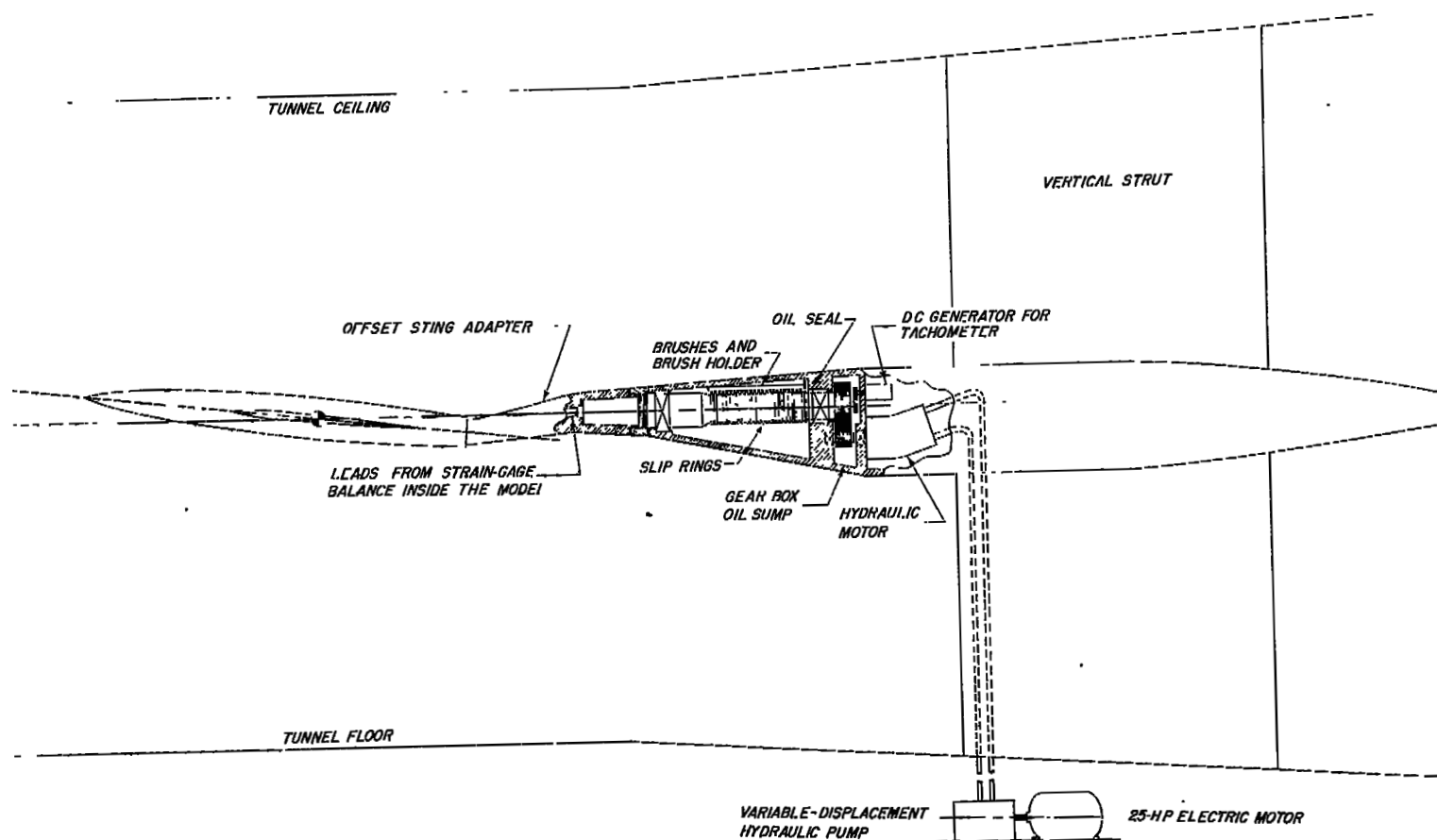


Figure 4.- General arrangement of forced-roll support system.

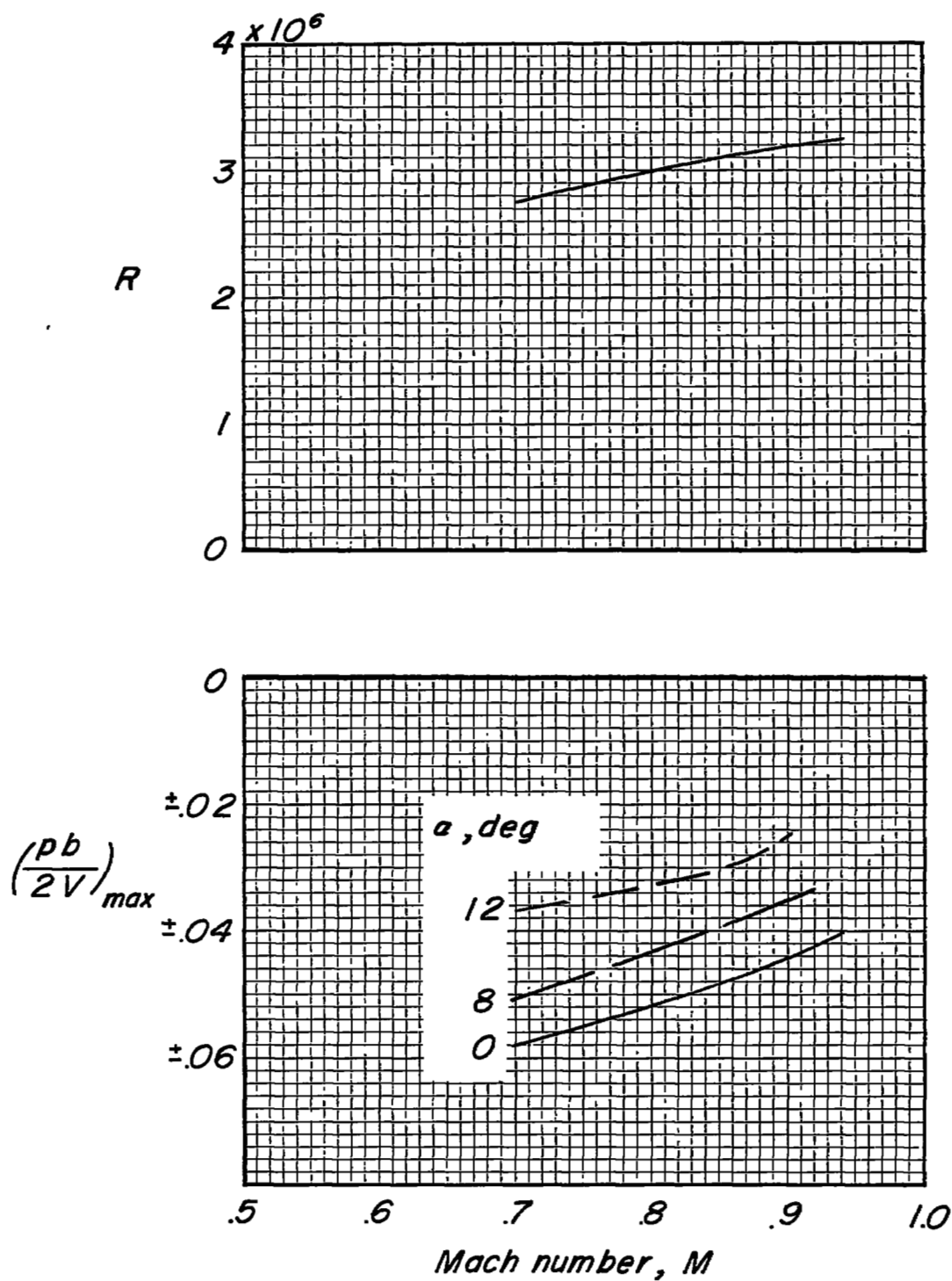


Figure 5.- Variation of maximum test $pb/2V$ and mean test Reynolds number with Mach number.

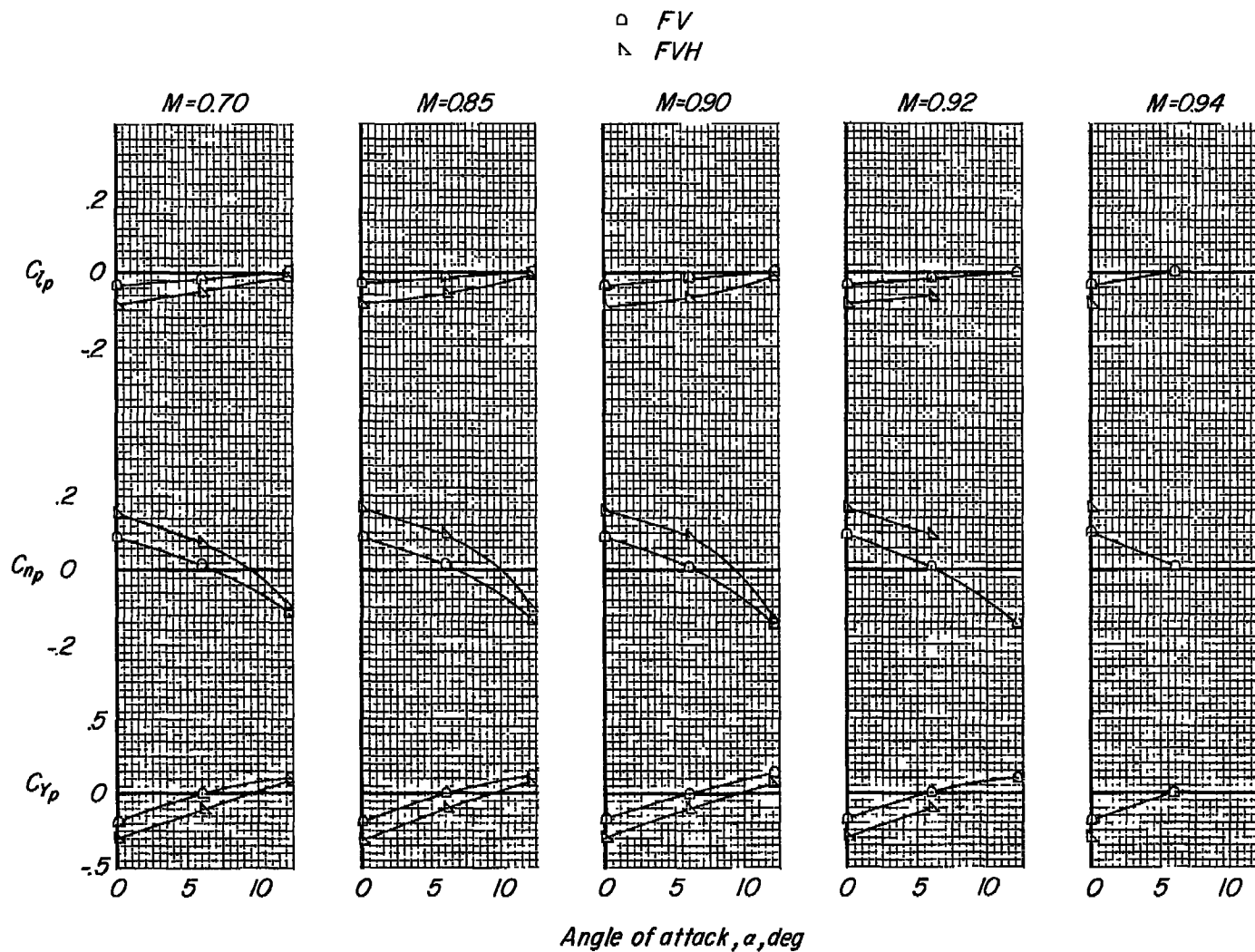


Figure 6.- Variation of rolling stability derivatives with angle of attack for the model without the wing, showing effects of the horizontal tail.

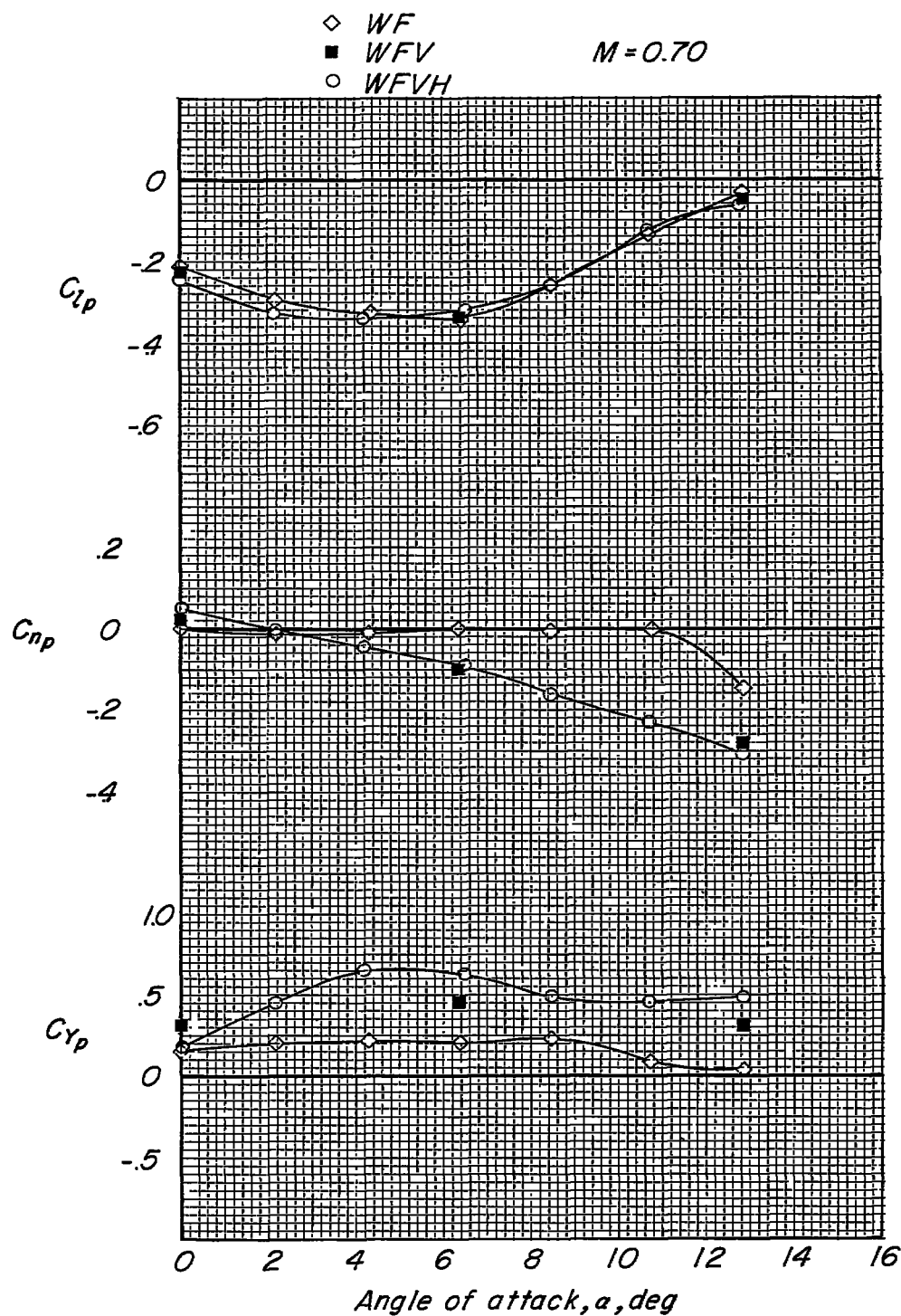


Figure 7.- Variation of rolling stability derivatives with angle of attack for the basic model showing the effects of the tail surfaces.

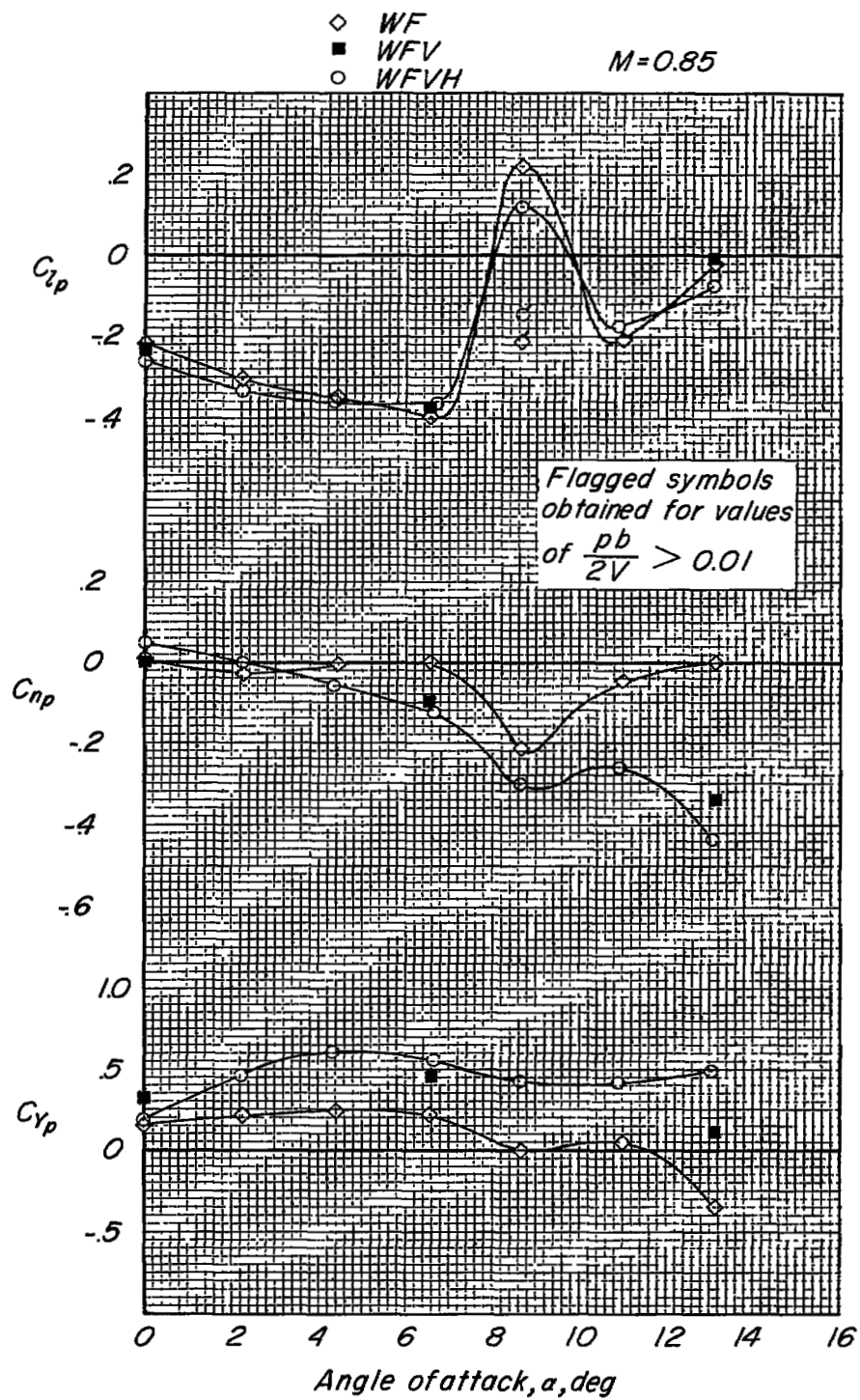


Figure 7.- Continued.

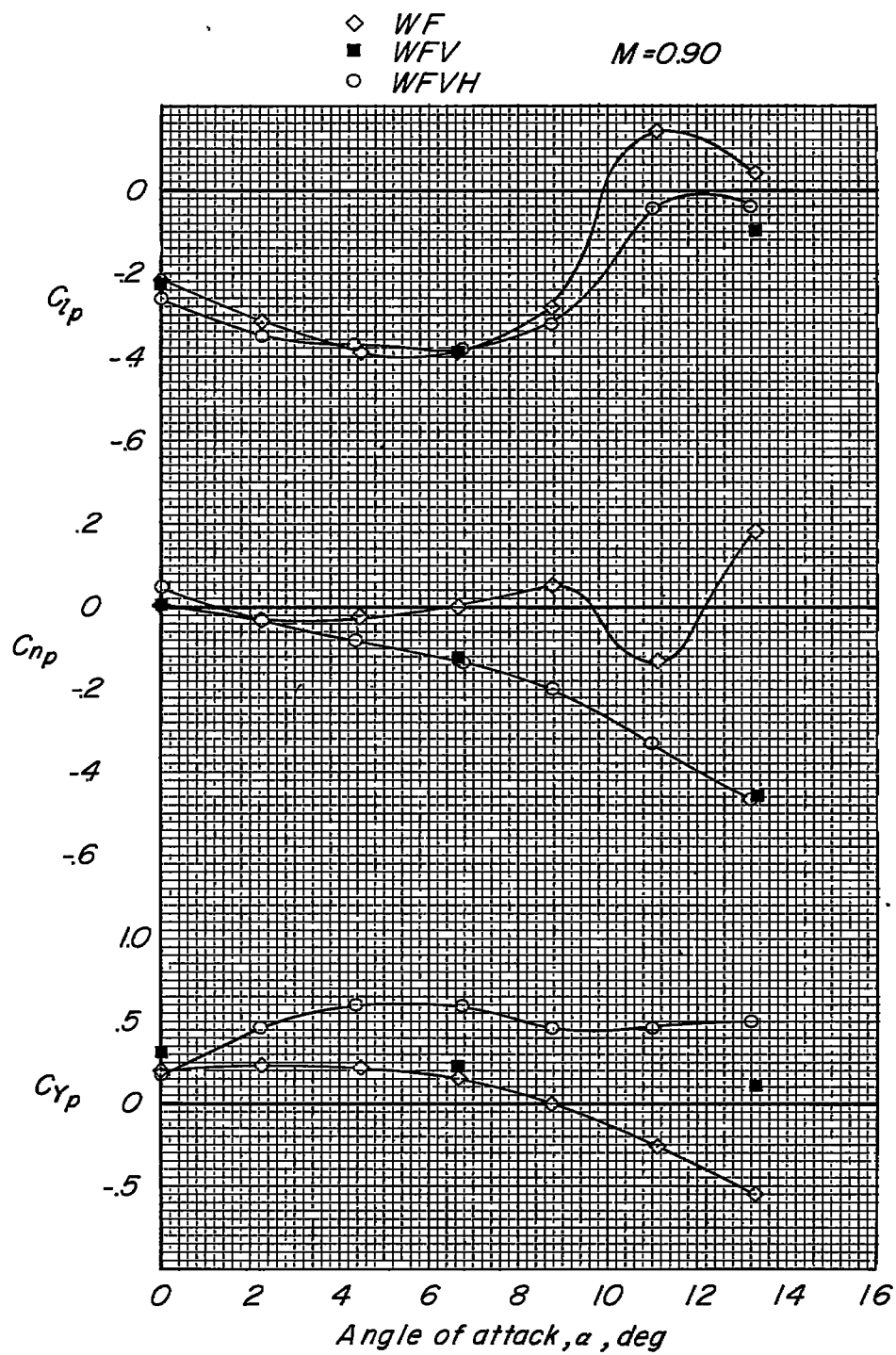


Figure 7.- Continued.

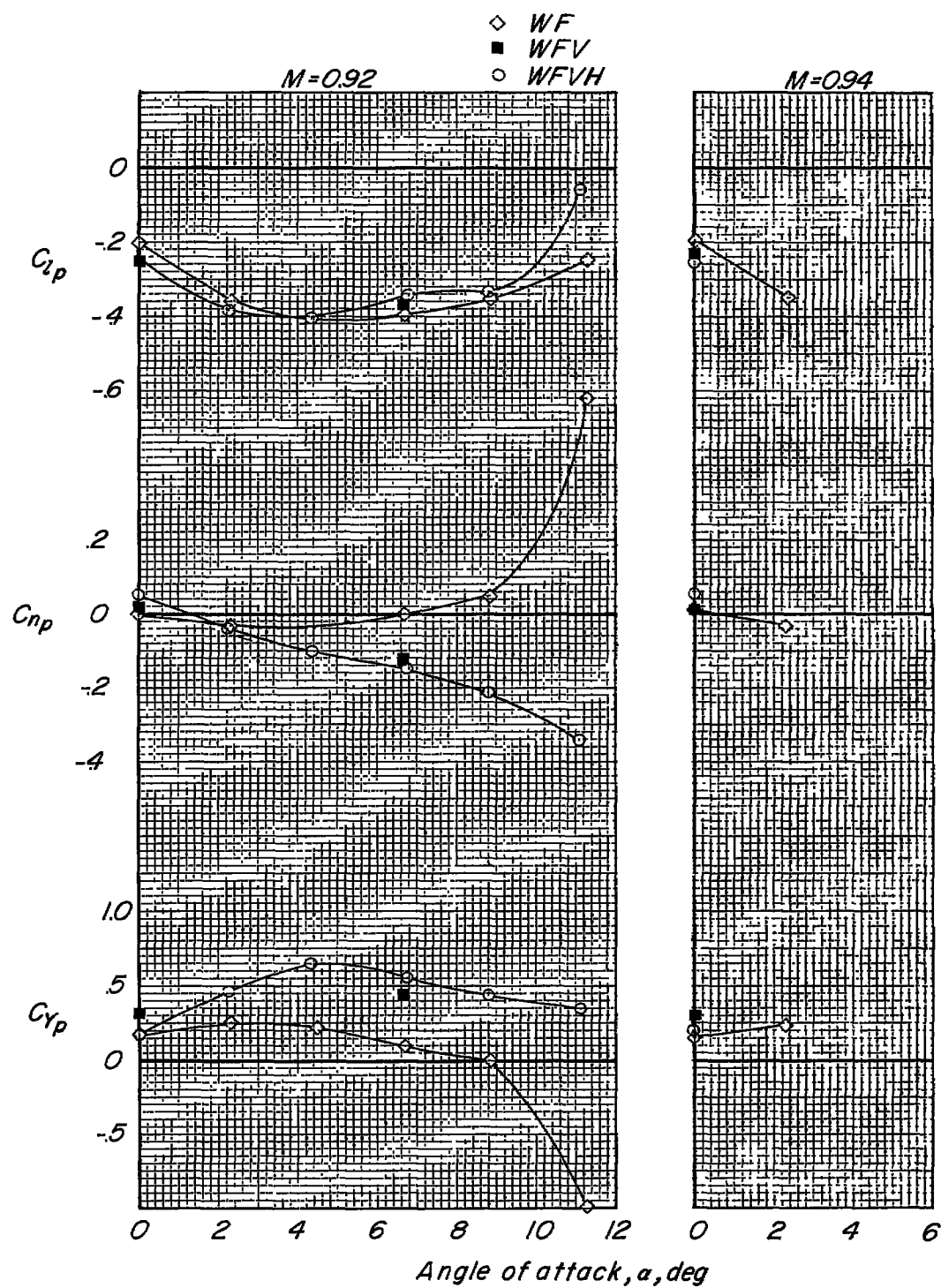


Figure 7.- Concluded.

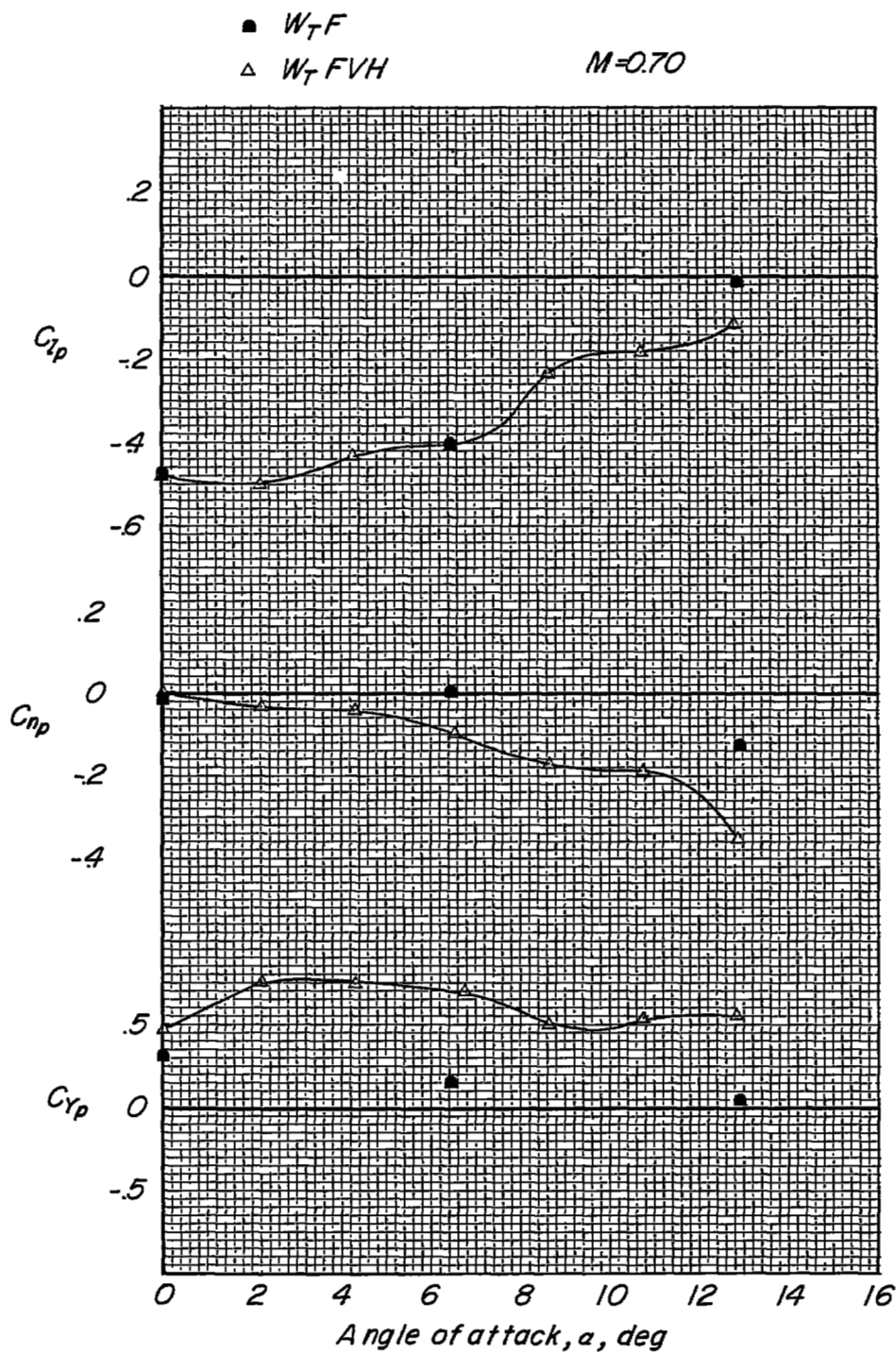


Figure 8.- Variation of rolling stability derivatives with angle of attack for the model with wing-tip tanks on.

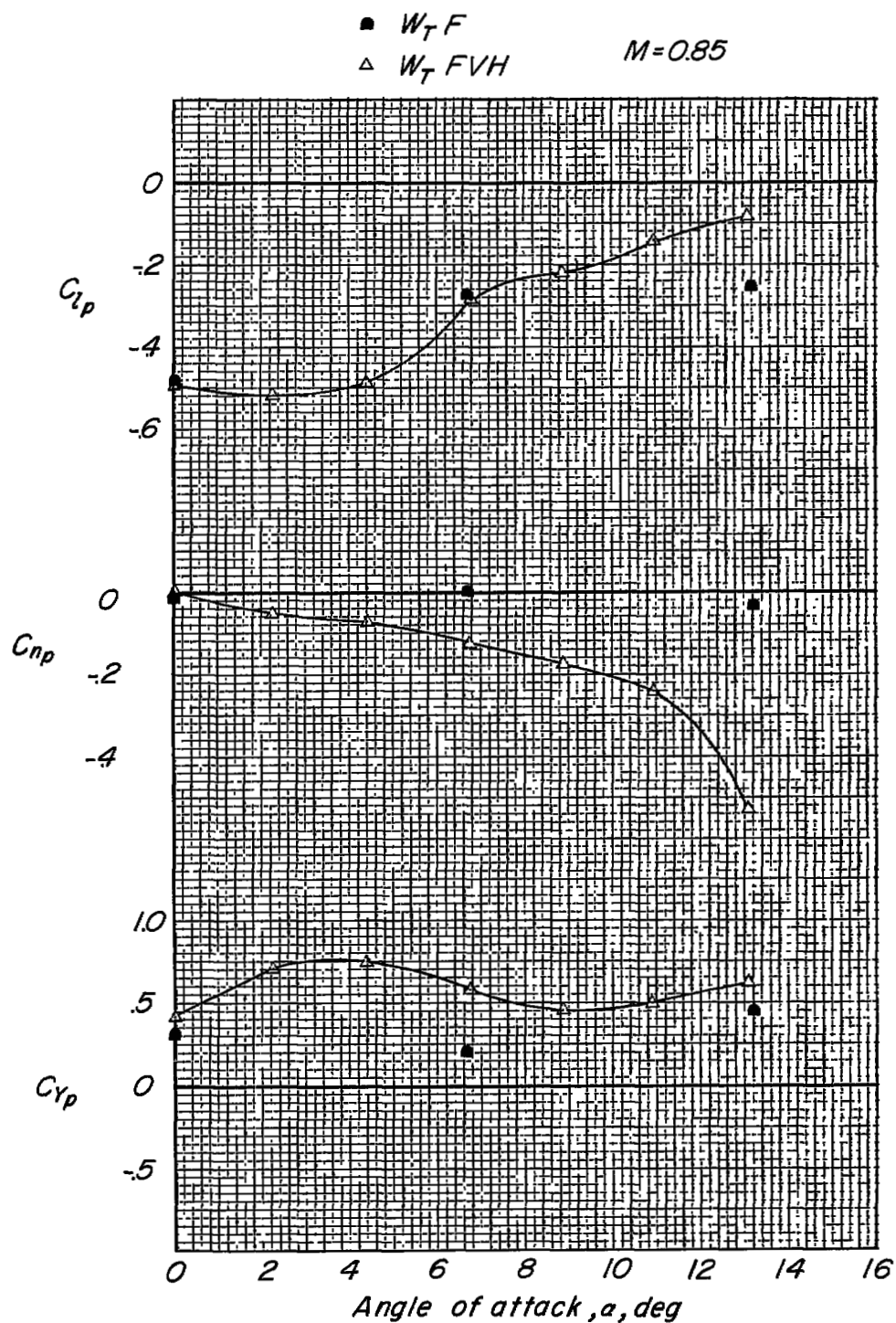


Figure 8.- Continued.

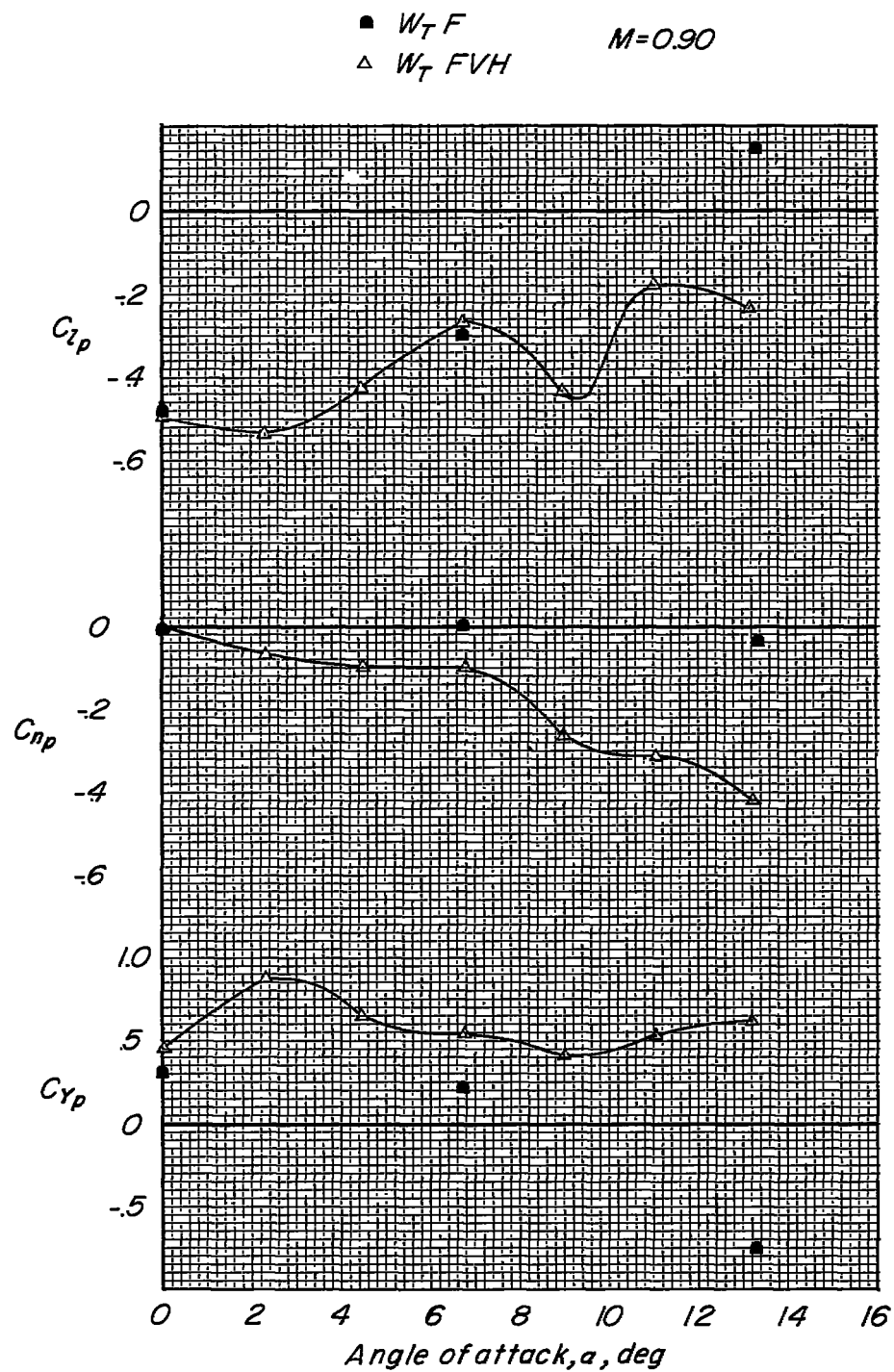


Figure 8.- Continued.

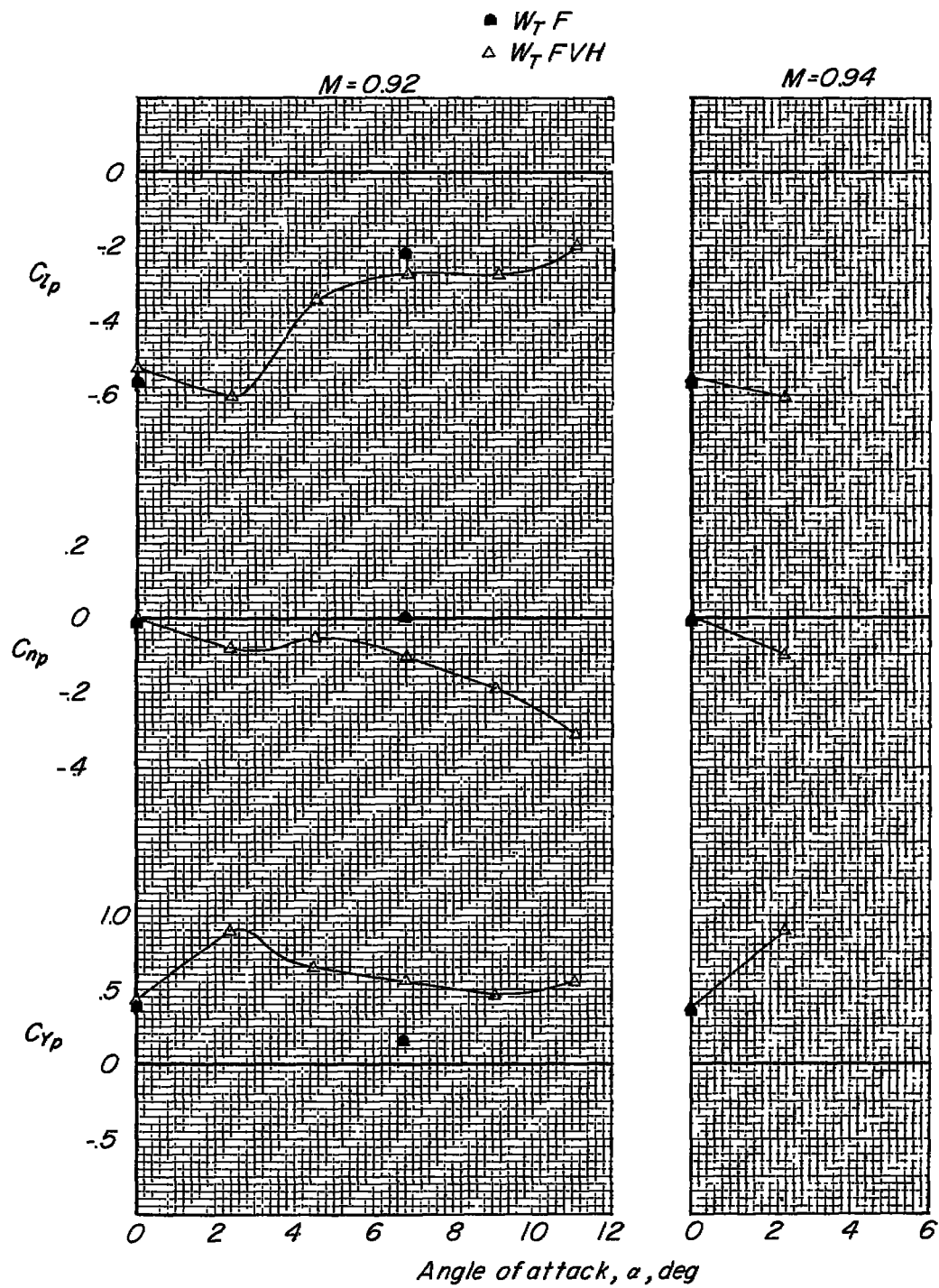


Figure 8.- Concluded.

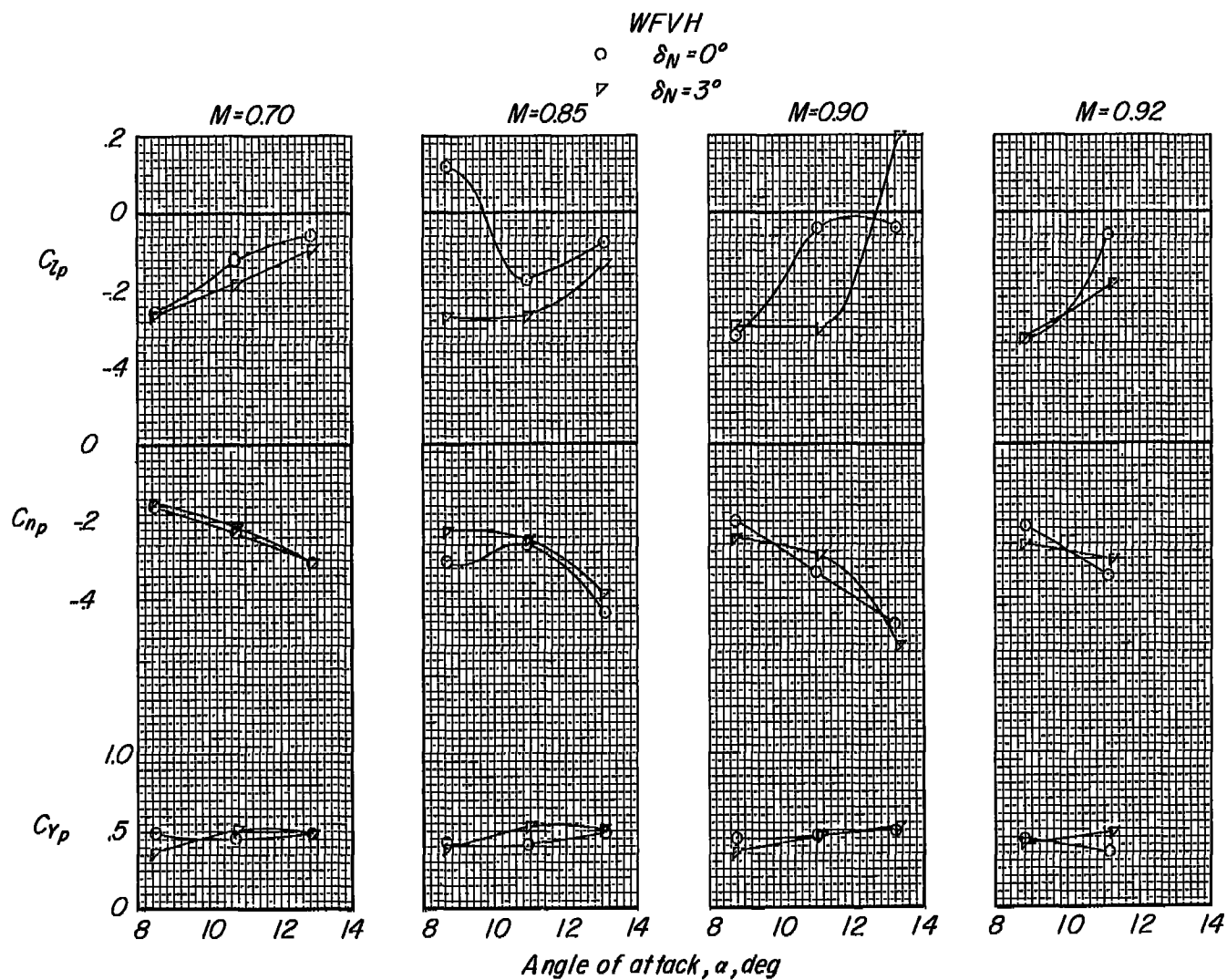


Figure 9.- Effect of leading-edge flap deflection on rolling stability derivatives of the model at the higher test angles of attack.

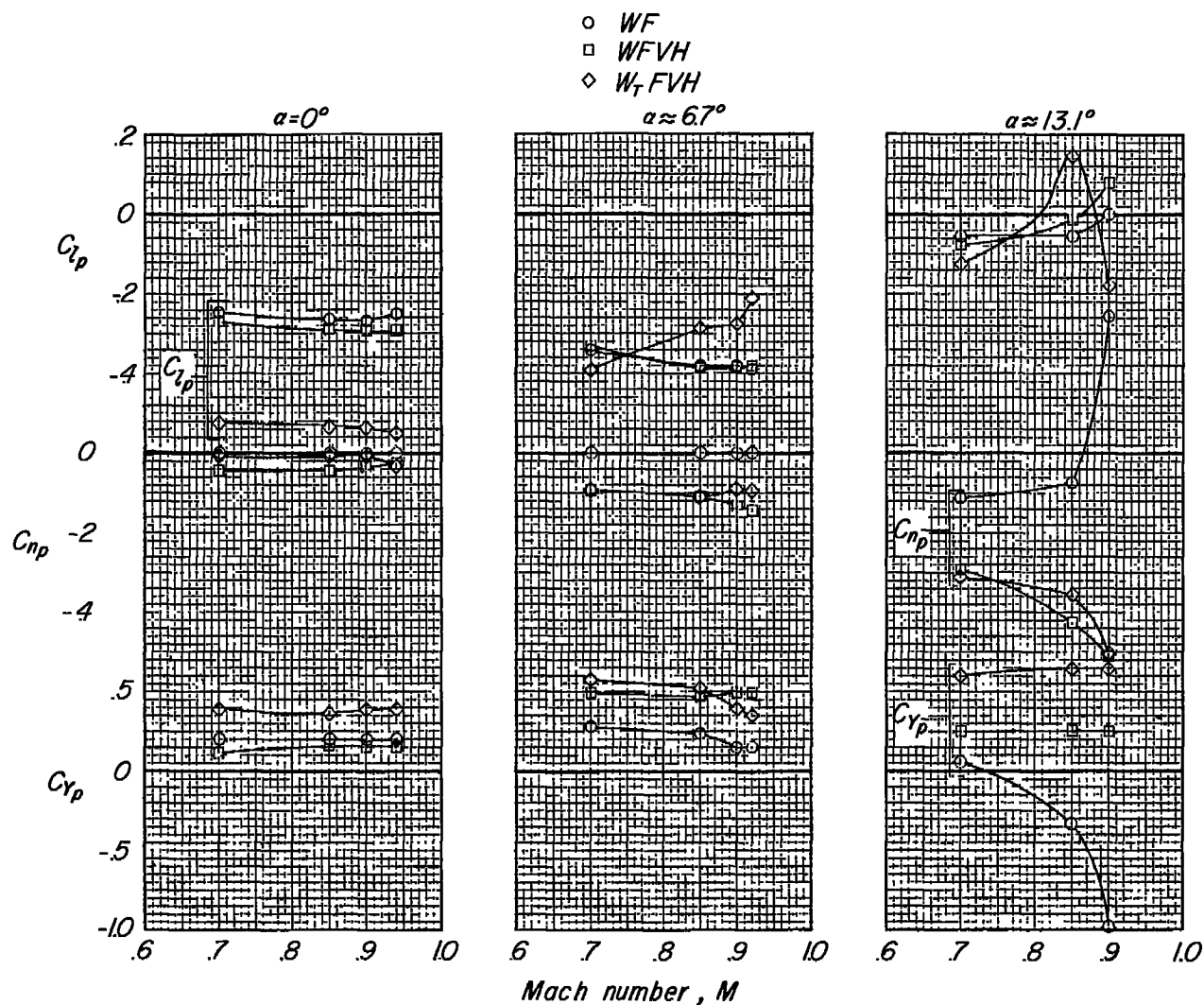


Figure 10.- Variation of rolling stability derivatives with Mach number for the model with ailerons deflected. $\delta_{a_T} = 15^\circ$.

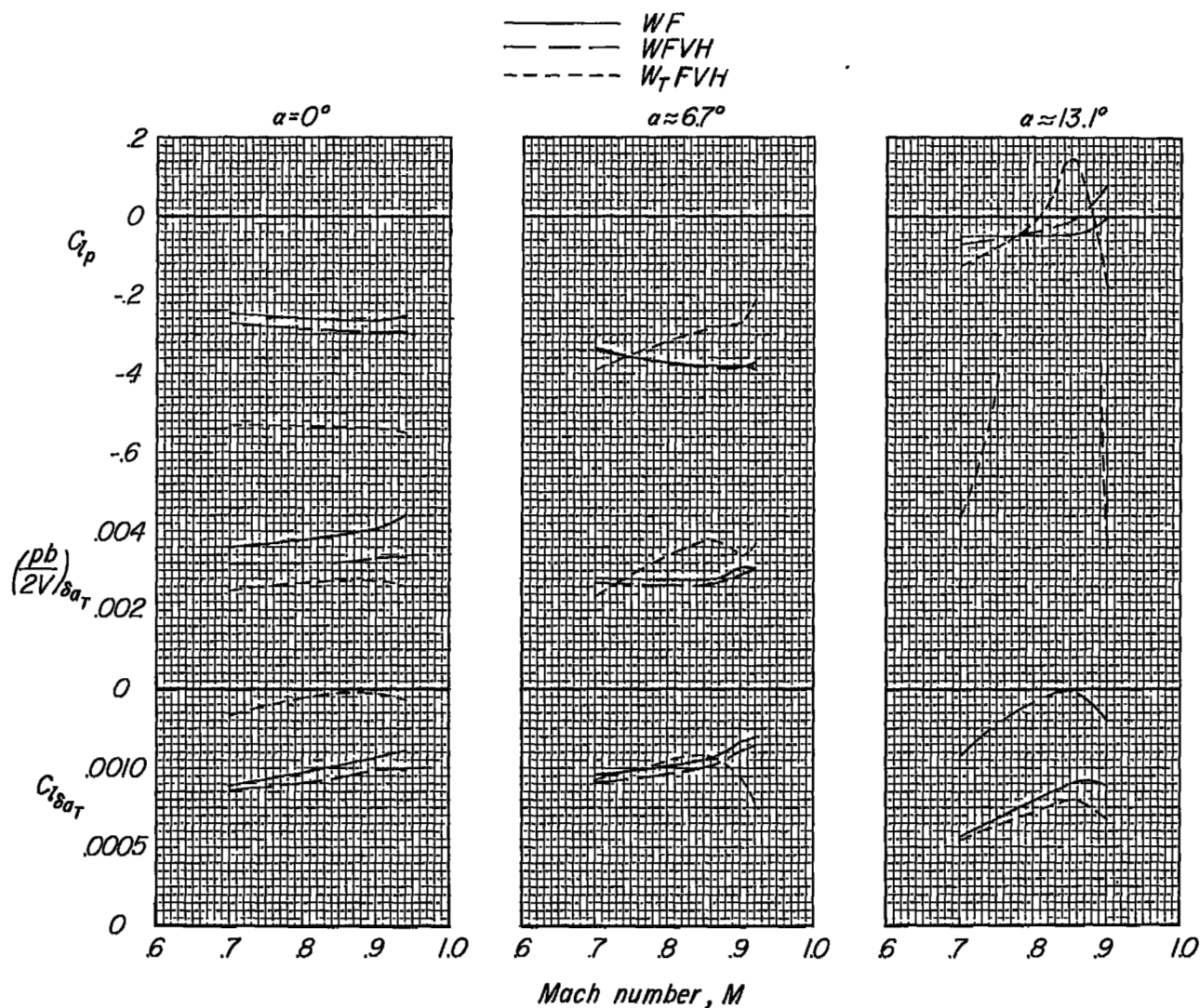


Figure 11.- Variation with Mach number of aileron effectiveness and rolling effectiveness obtained from tests of the model with ailerons deflected.

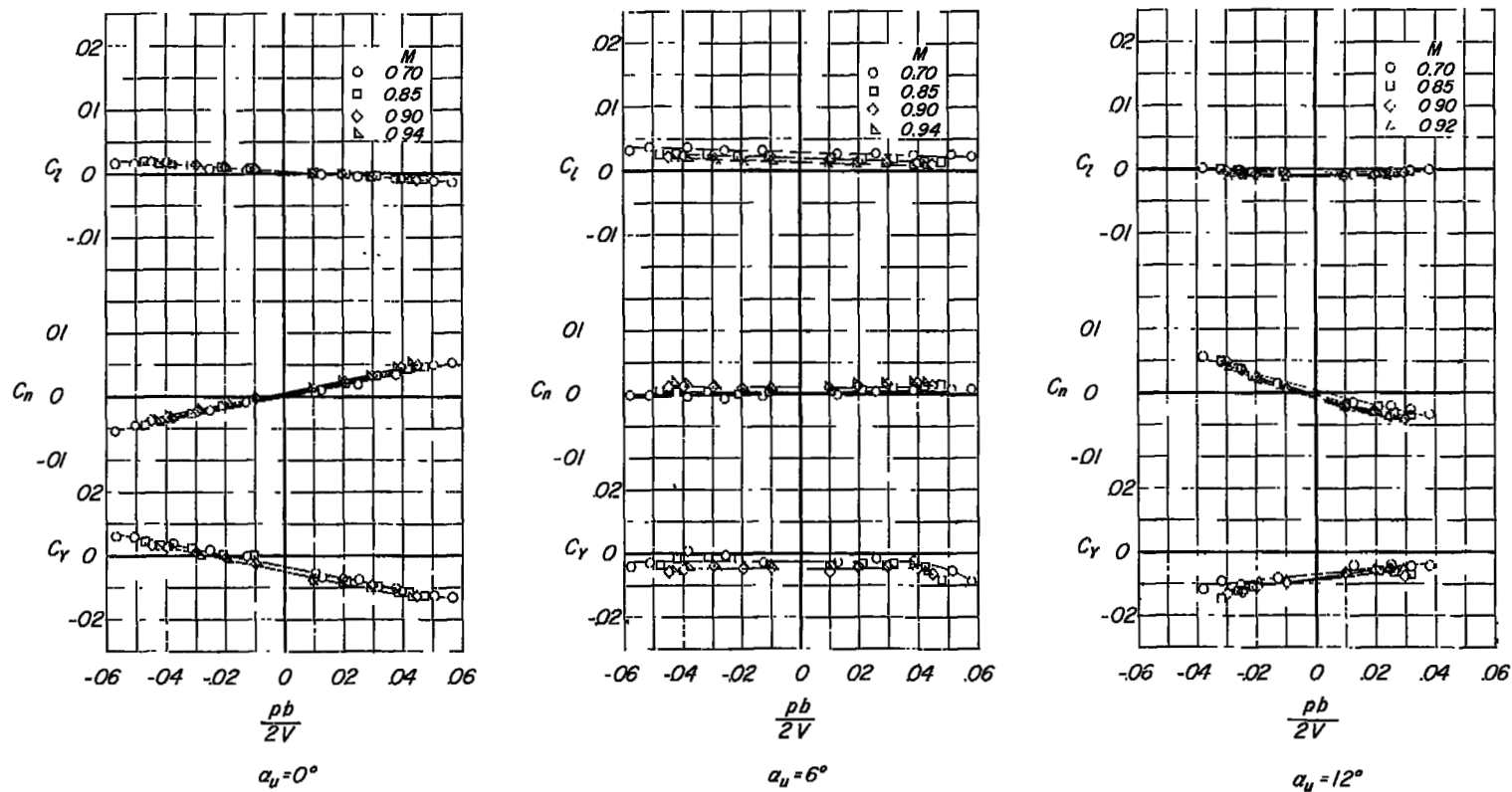


Figure 12.- Variation of lateral characteristics of the model with wing-tip helix angle. Configuration FV.

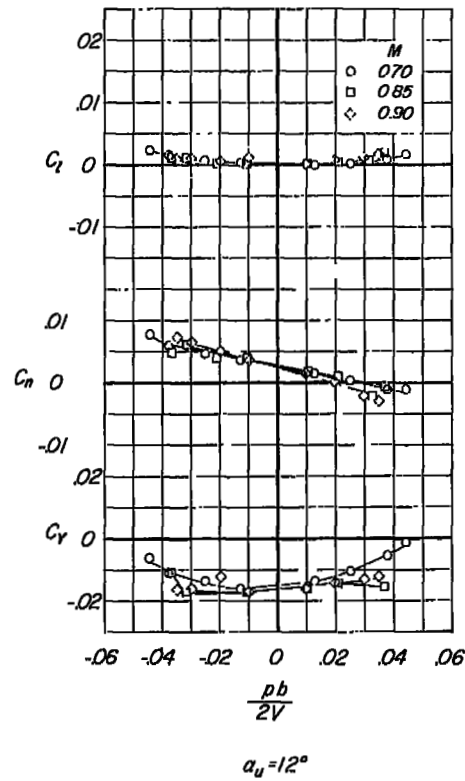
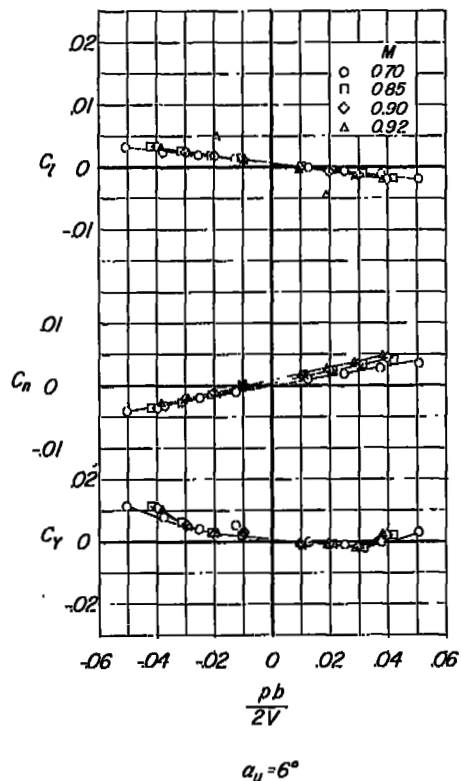
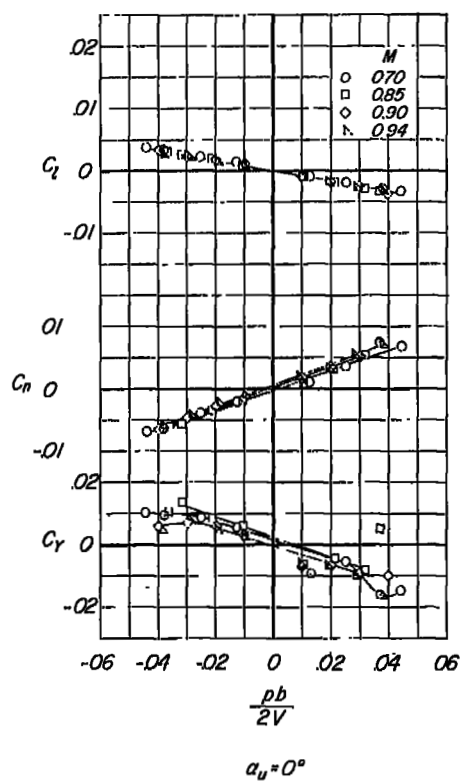


Figure 13.- Variation of lateral characteristics of the model with wing-tip helix angle. Configuration FVH.

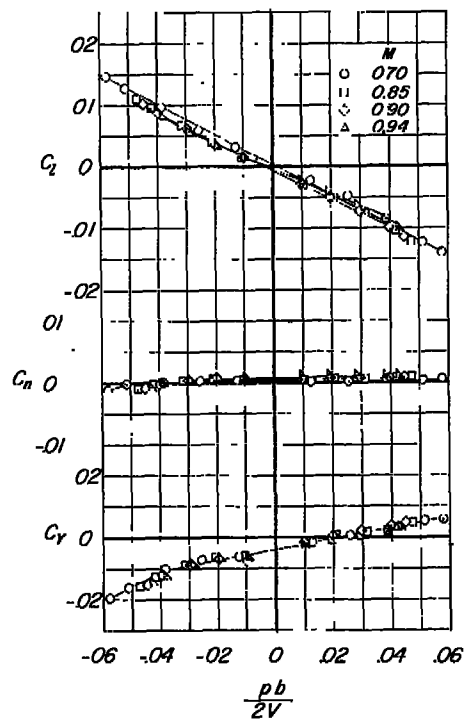
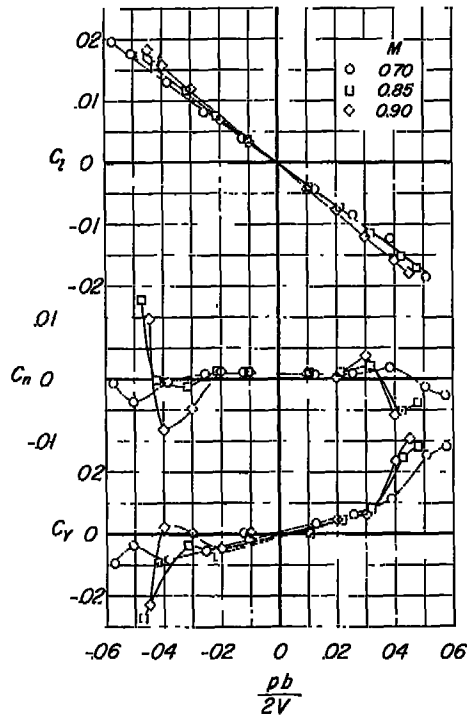
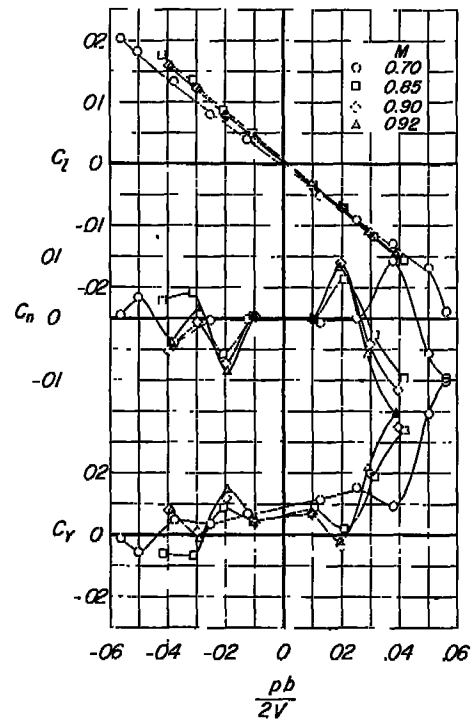

 $a_u = 0^\circ$

 $a_u = 4^\circ$

 $a_u = 6^\circ$

Figure 14.- Variation of lateral characteristics of the model with wing-tip helix angle. Configuration WF.

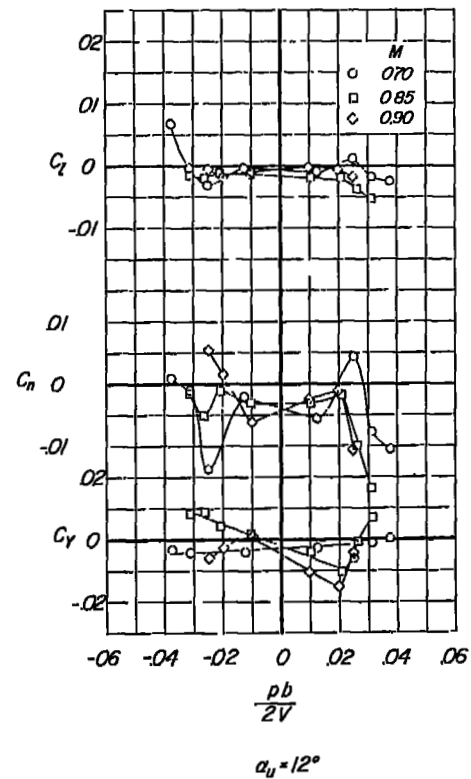
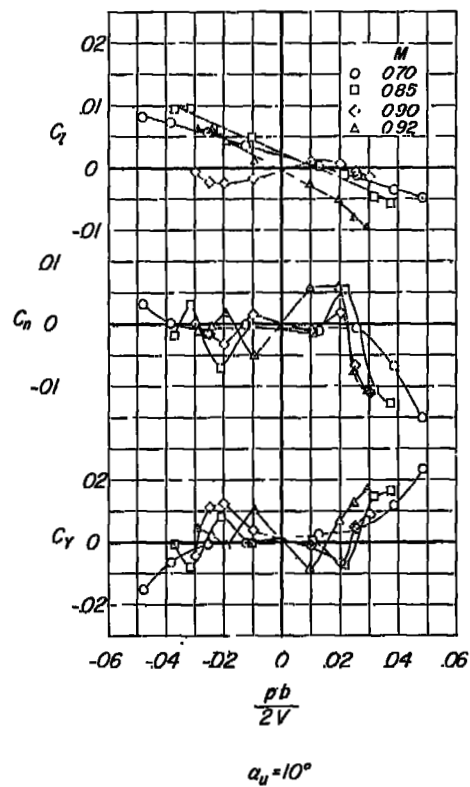
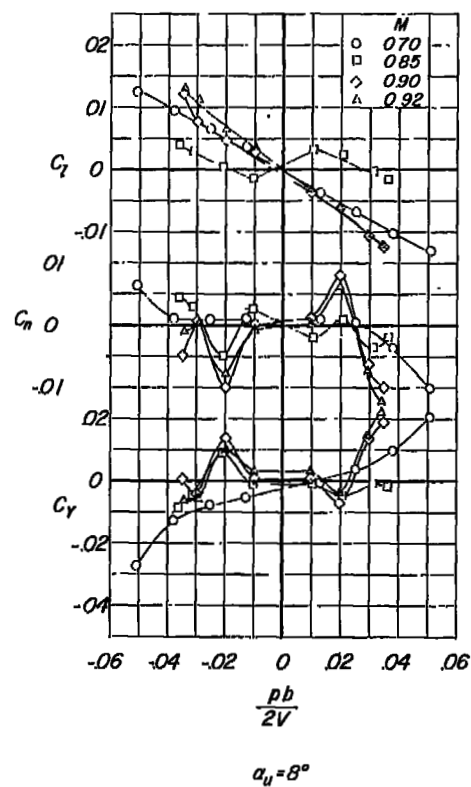


Figure 14.- Concluded.

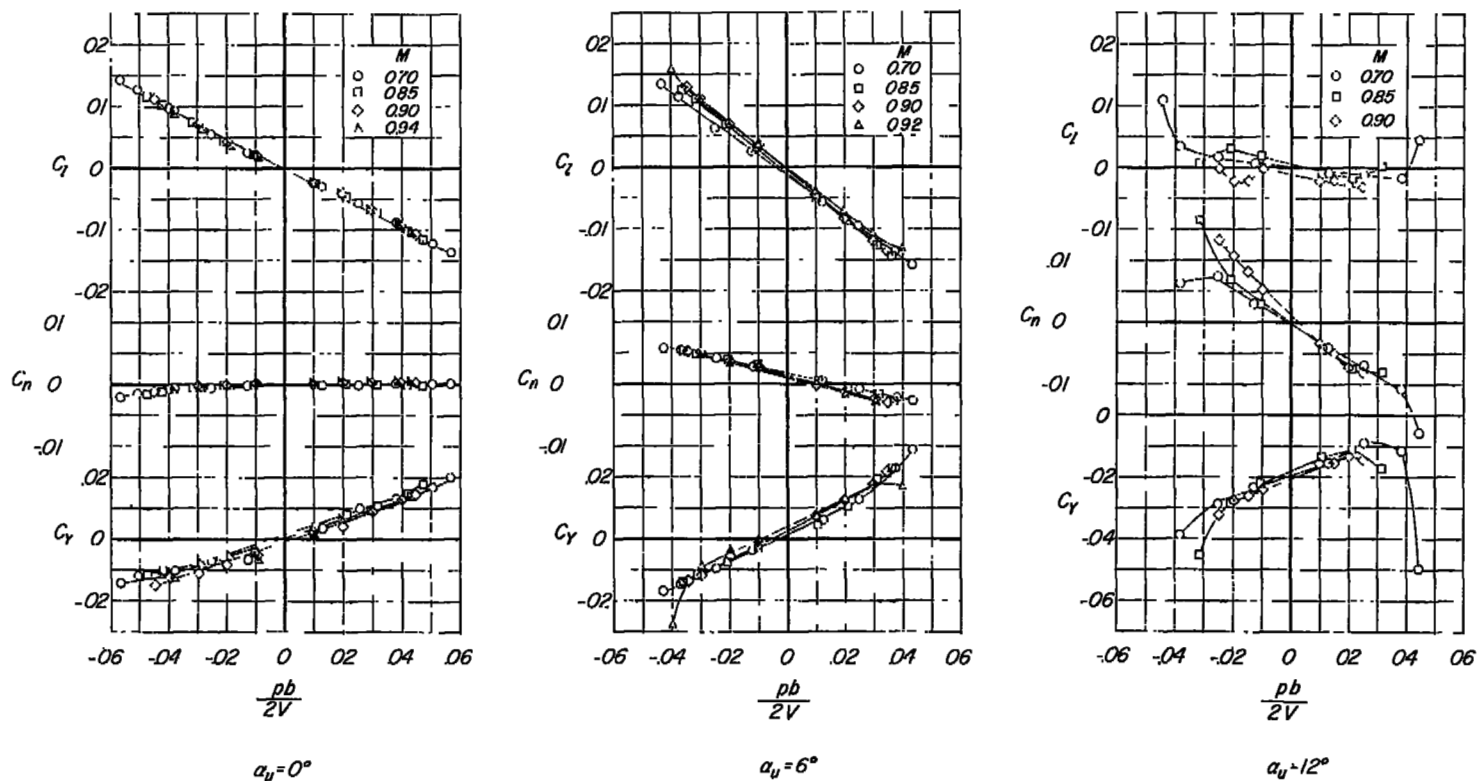


Figure 15.- Variation of lateral characteristics of the model with wing-tip helix angle. Configuration WFV.

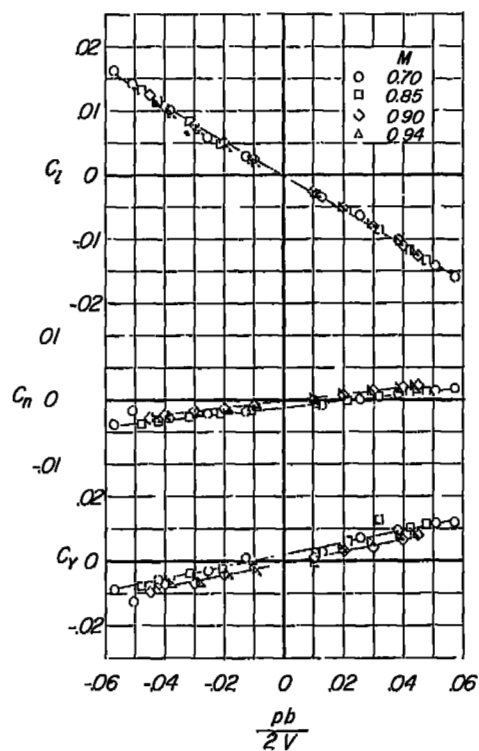
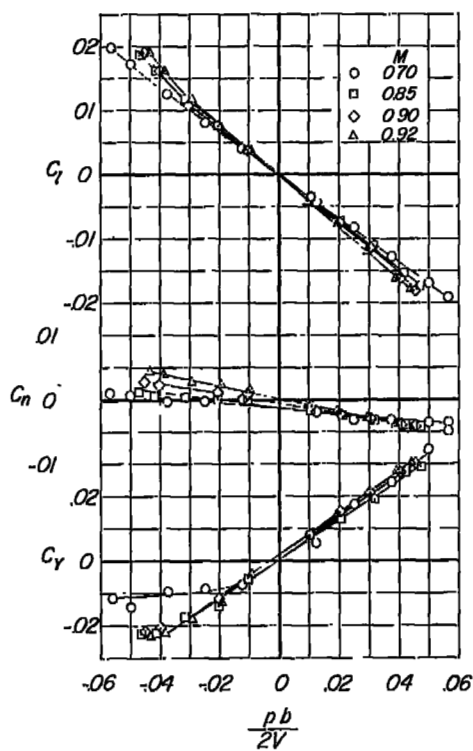
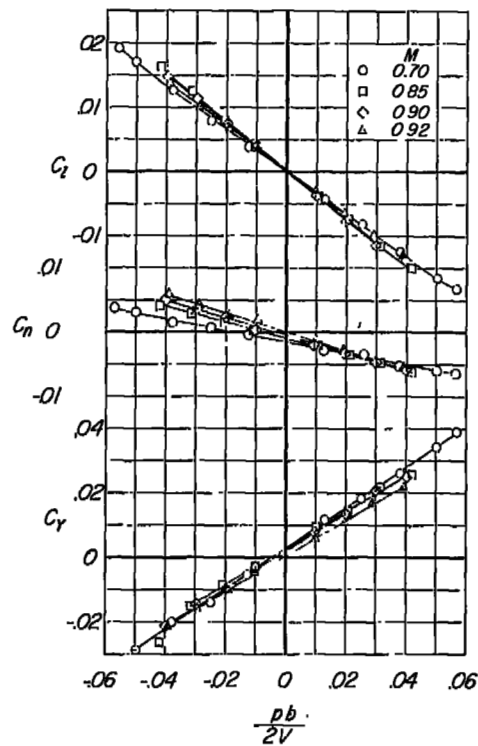
 $\alpha_u = 0^\circ$  $\alpha_u = 4^\circ$  $\alpha_u = 6^\circ$

Figure 16.- Variation of lateral characteristics of the model with wing-tip helix angle. Configuration WFWII.

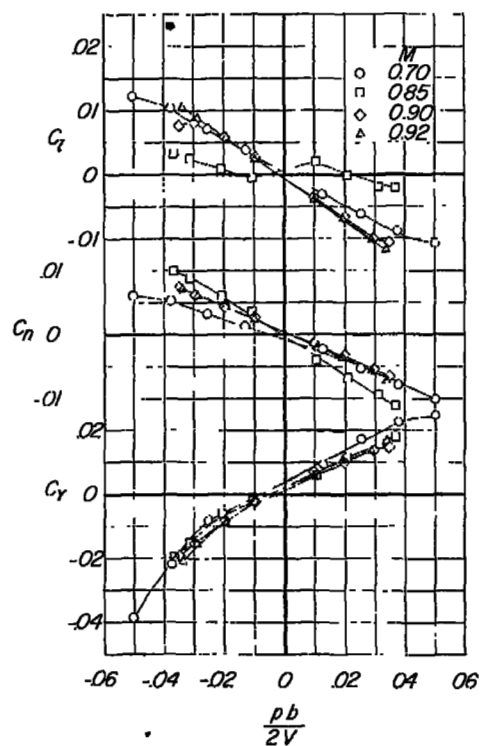
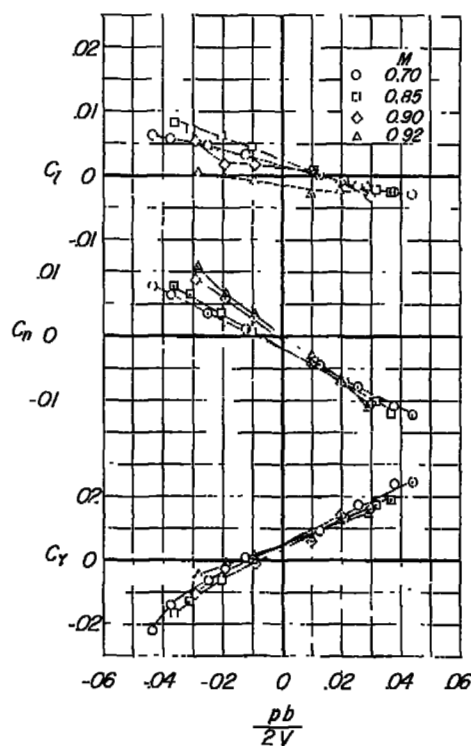
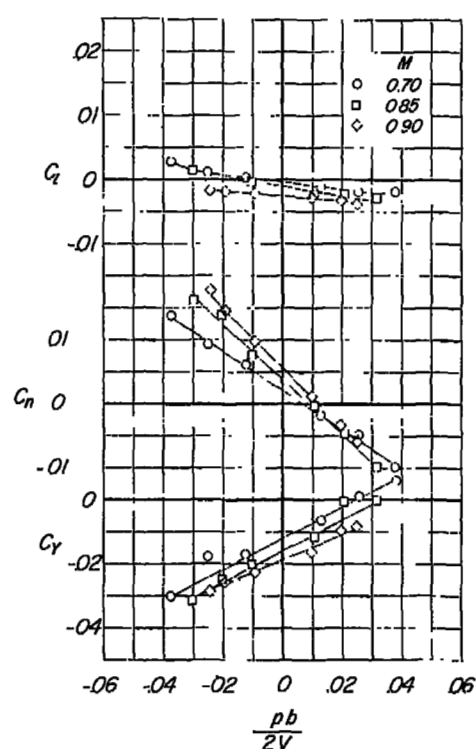
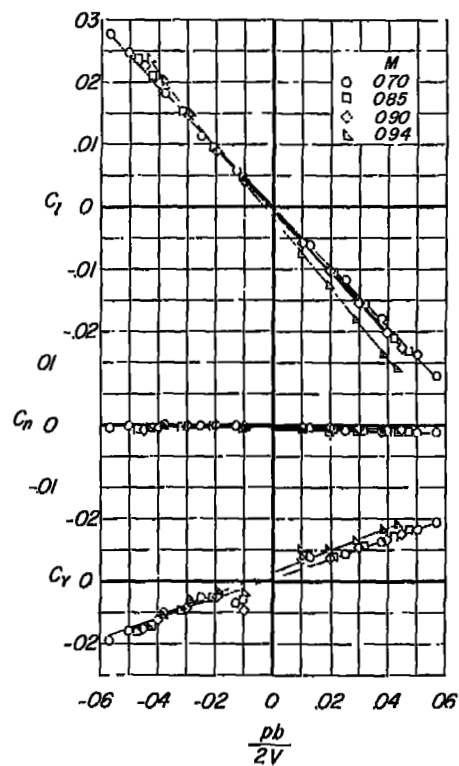
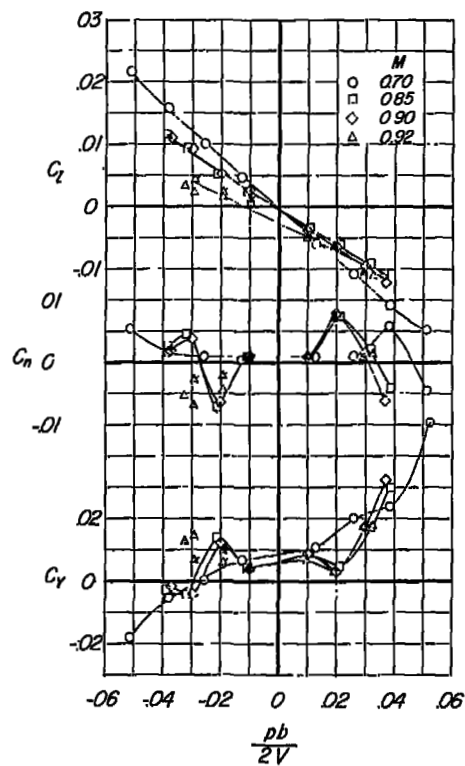

 $\alpha_u = 8^\circ$

 $\alpha_u = 10^\circ$

 $\alpha_u = 12^\circ$

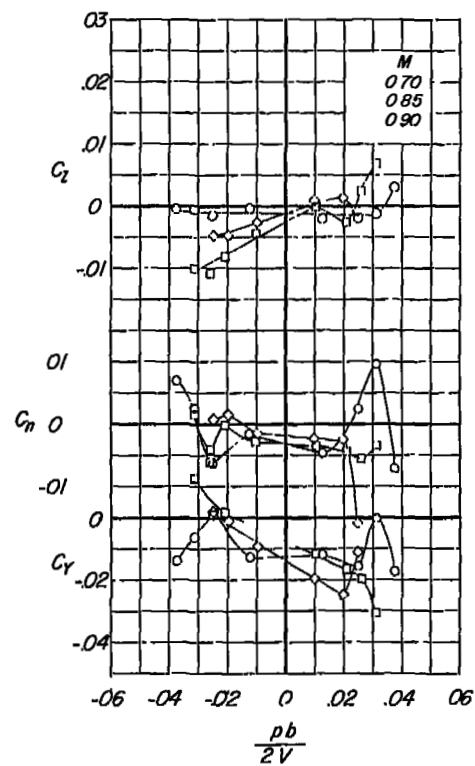
Figure 16.- Concluded.



$\alpha_u = 0^\circ$



$\alpha_u = 6^\circ$



$\alpha_u = 12^\circ$

(a) Configuration W_{TF}.

Figure 17.- Variation with wing-tip helix angle of lateral characteristics of the model with tanks on.

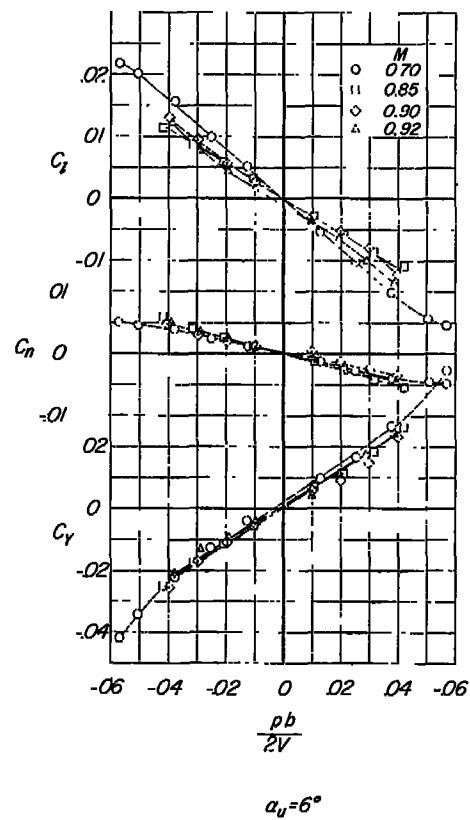
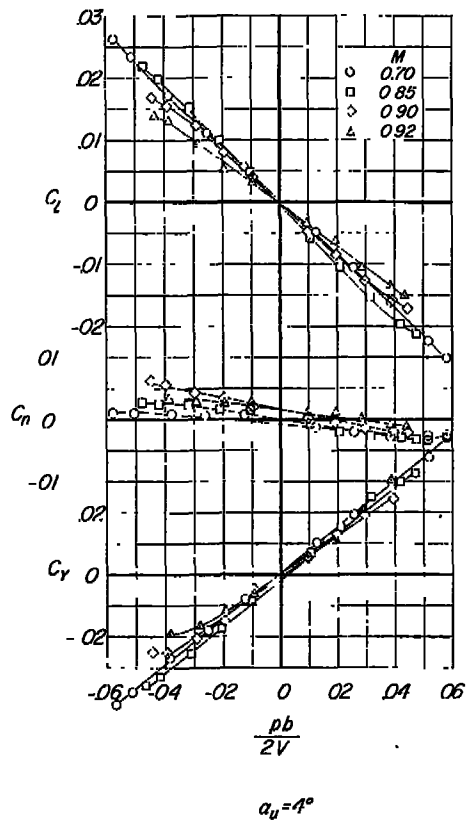
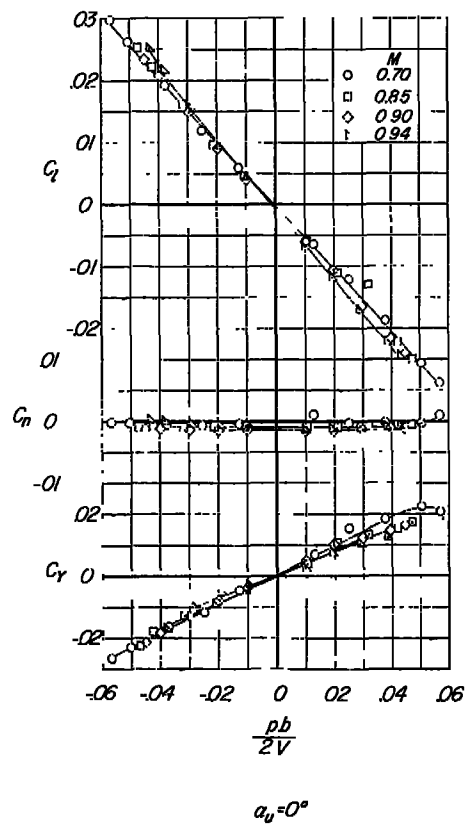
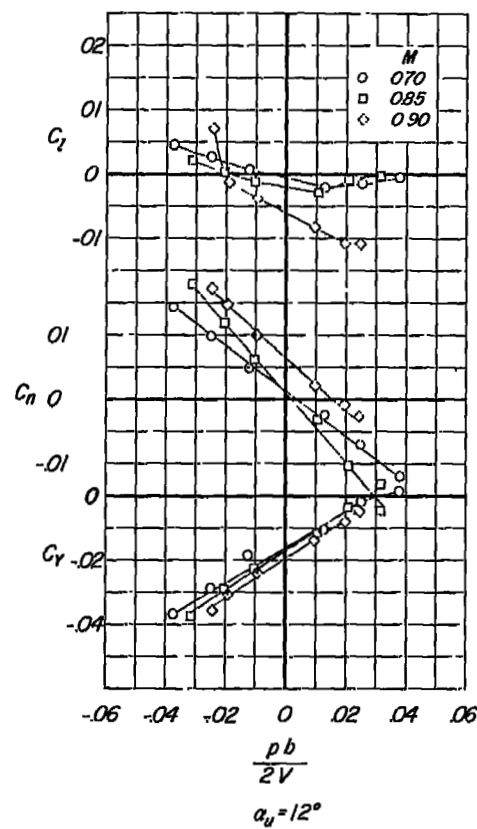
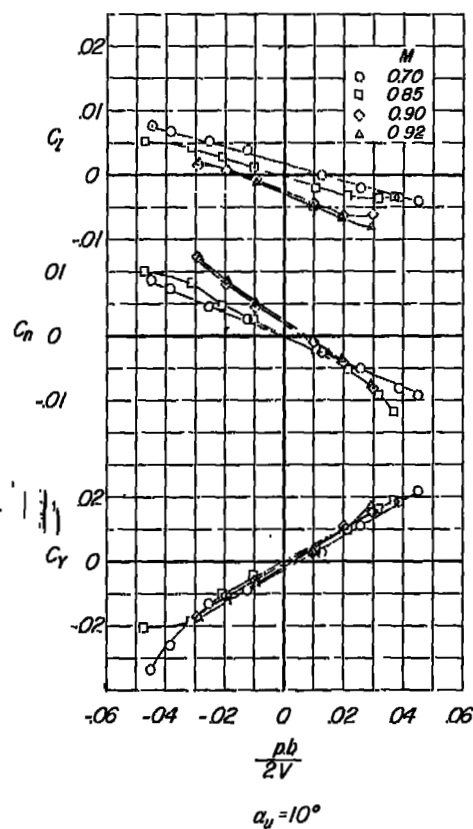
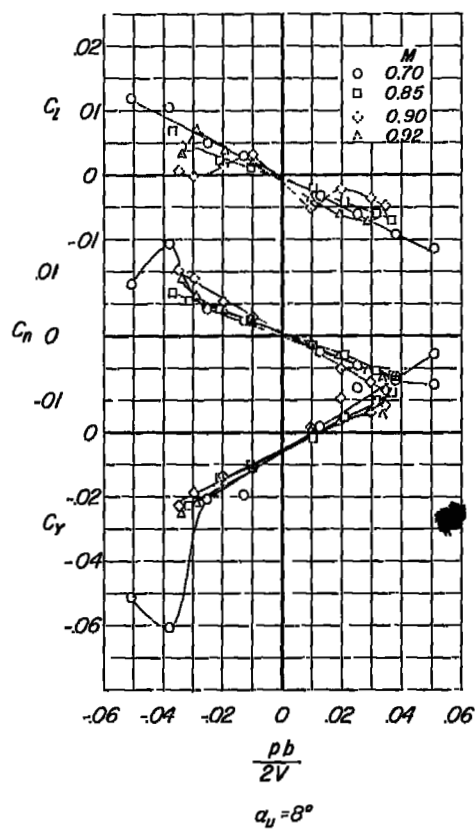
(b) Configuration $W_T FVH$.

Figure 17.- Continued.



(b) Concluded.

Figure 17.- Concluded.

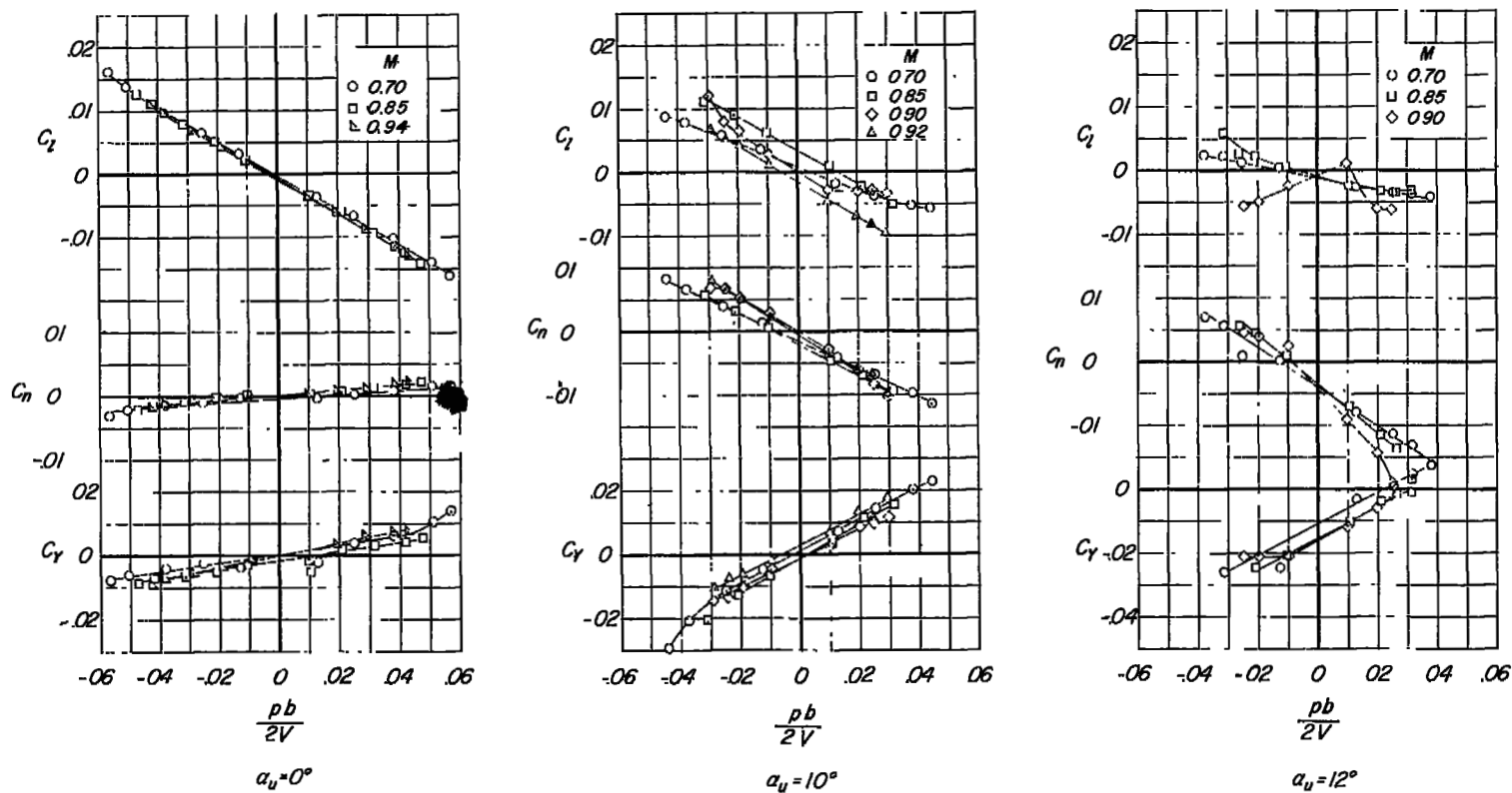
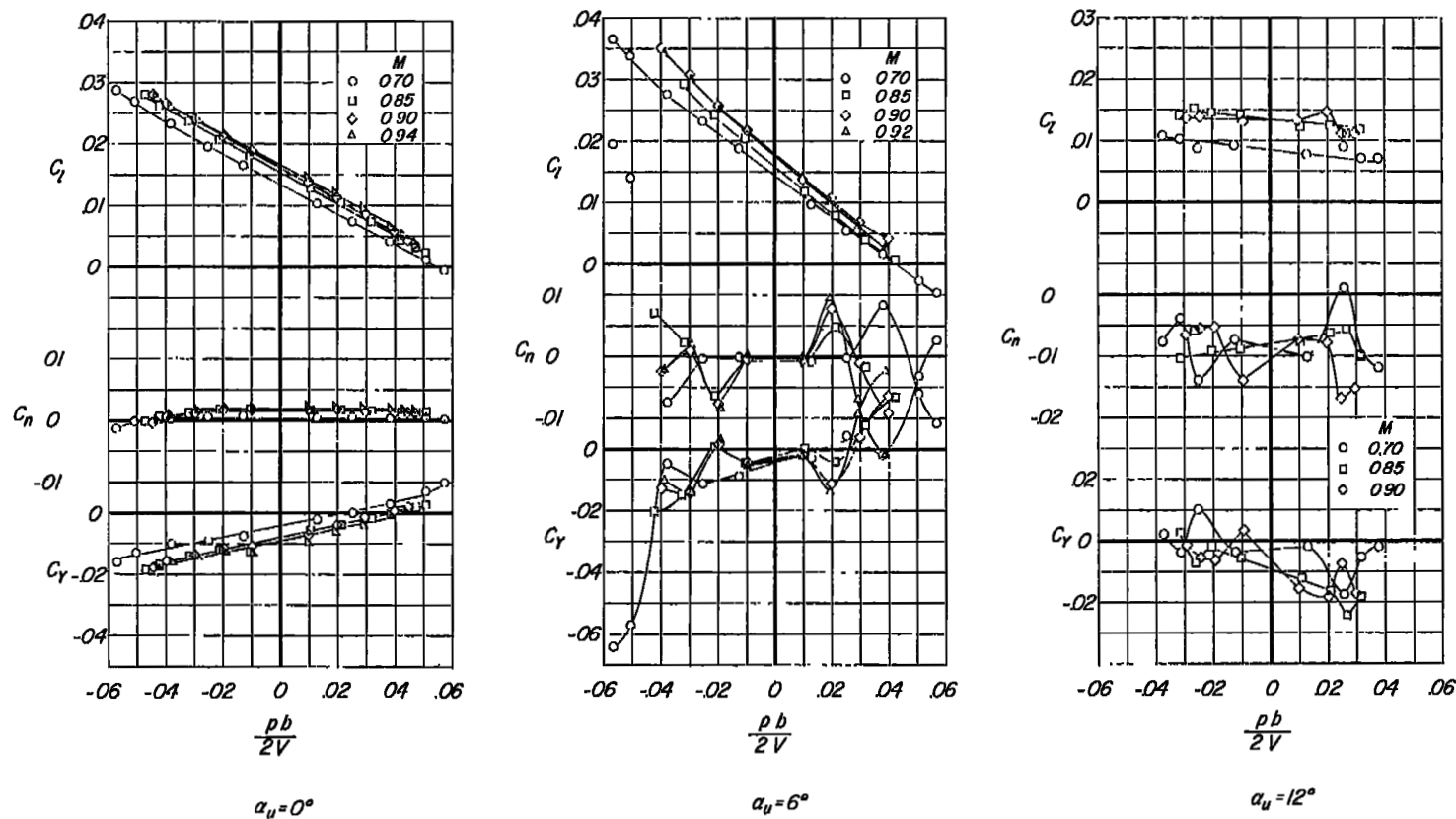
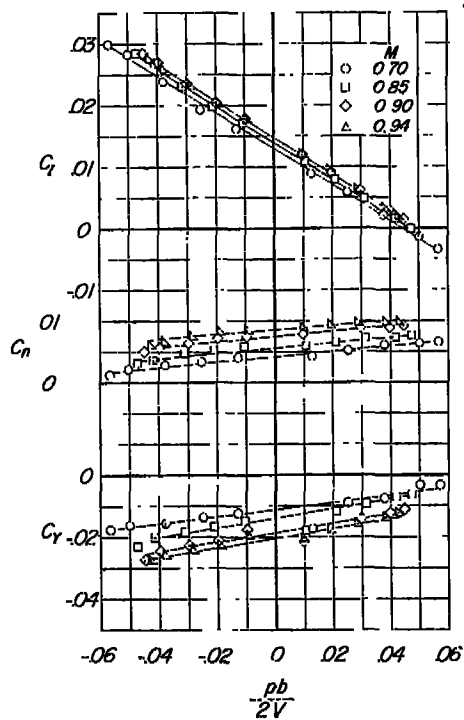


Figure 18.- Variation with wing-tip helix angle of lateral characteristics of the model with leading-edge flaps deflected. Configuration WFWH.

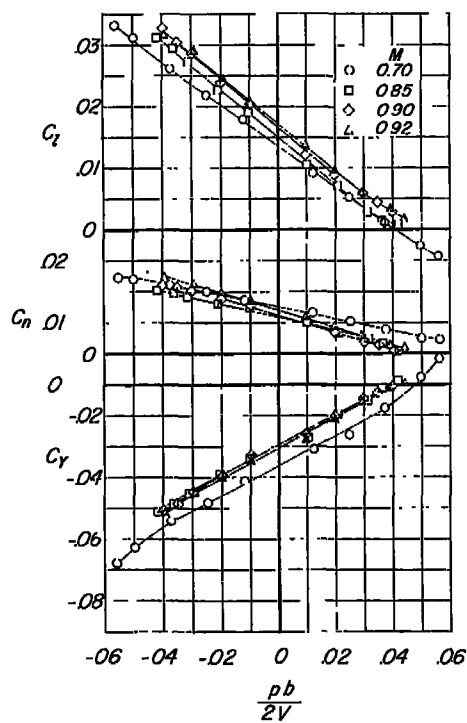


(a) Configuration WF.

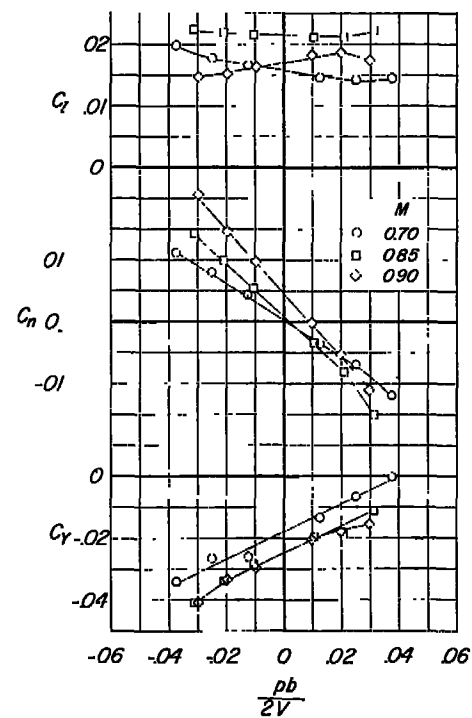
Figure 19.- Variation with wing-tip helix angle of lateral characteristics of the model with ailerons deflected. $\delta_{a_T} = 15^\circ$.



$\alpha_u = 0^\circ$



$\alpha_u = 6^\circ$



$\alpha_u = 12^\circ$

(b) Configuration WFWH.

Figure 19.- Continued.

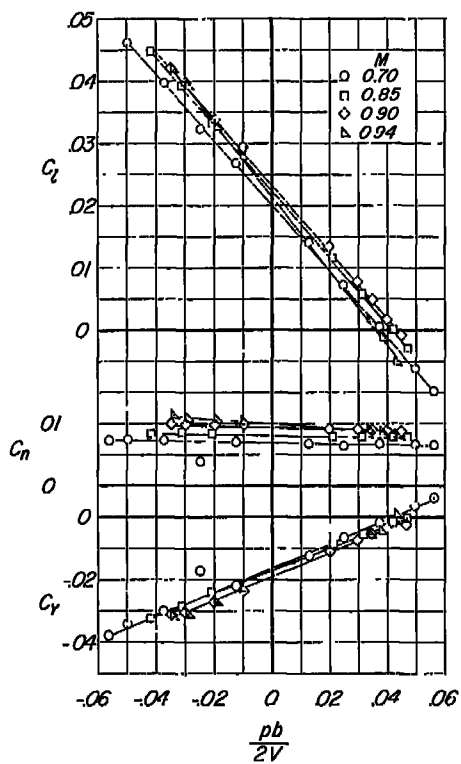
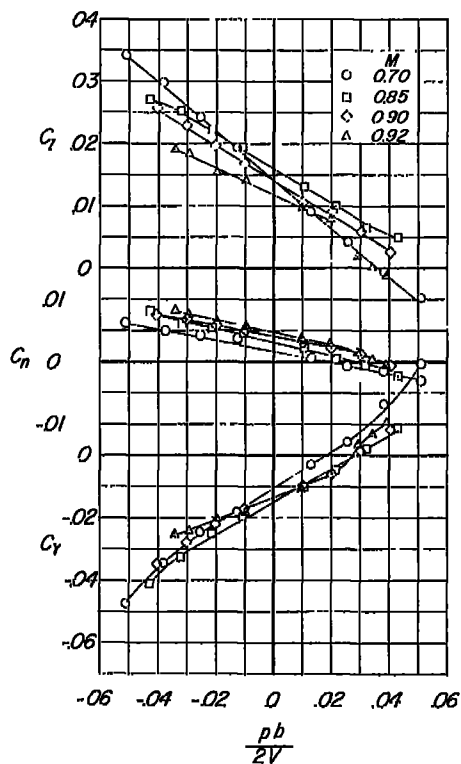
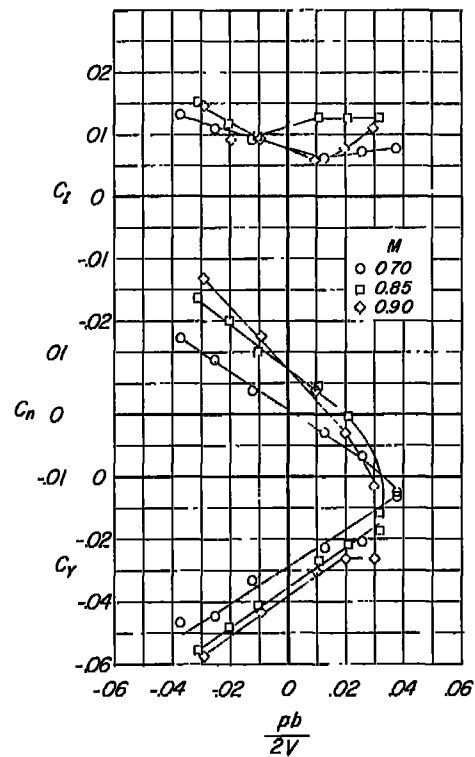
 $\alpha_u = 0^\circ$  $\alpha_u = 6^\circ$  $\alpha_u = 12^\circ$ (c) Configuration W_{TFVH} .

Figure 19.- Concluded.

[REDACTED]

NASA Technical Library
3 1176 01437 1786

[REDACTED]

1
1

1
1

1
1

[REDACTED]

[REDACTED]